Master's Thesis

Design and Characterization of Heteroaromatic π-Conjugated Semiconducting Materials

Daehee Han

Department of Energy Engineering

(Energy Engineering)

Graduate School of UNIST

2018

Design and Characterization of Heteroaromatic

π-Conjugated Semiconducting Materials

Daehee Han

Department of Energy Engineering

(Energy Engineering)

Graduate School of UNIST

Design and Characterization of Heteroaromatic

π-Conjugated Semiconducting Materials

A thesis/dissertation

submitted to the Graduate School of UNIST

in partial fulfillment of the

requirements for the degree of

Master of Science

Daehee Han

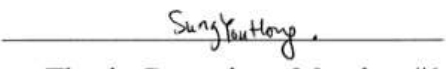12/05/2017of submission

Approved by

_____

Advisor

Changduk Yang

Design and Characterization of Heteroaromatic

π-Conjugated Semiconducting Materials

Daehee Han

This certifies that the thesis/dissertation of Daehee Han is approved.

12/05/2017

signature

Advisor: Changduk Yang

signature

Sung You Hong: Thesis Committee Member #1

signature

Hyesung Park: Thesis Committee Member #2

Abstract

Over the past few decades, π-conjugated molecules have been attended due to the exotic properties and widely used for the devices such as organic photovoltaics (OPVs), field effect transistors (FETs) and light emitting diodes (LEDs). Especially, π-conjugated frameworks of fused aromatic compounds incorporated with heteroatoms exhibited distinguishable features such like high electron affinity and strengthen intermolecular interaction without significant steric effect. Among of previously reported frameworks, dithienosilole (DTSi) and dithienogermole (DTGe) have been considered as one of the outstanding π-conjugated molecules.

In this contribution, I investigated study about the effects of introducing the cyclic chain onto the fused heteroaromatic compounds with comparisons of heteroaromatic compounds incorporating non-cyclic chain **in chapter 1**. Furthermore, I synthesized these two types of π-conjugated molecules depends on central heteroatom with characterization and investigated optoelectrical, electrochemical properties and crystalline structure of thin film. And then, these four π-conjugated molecules applied finally as a donor material of OPVs.

In chapter 2, effects of introducing fluorine atom (F) on different position in benzothiadiazole (BT) unit with different end capping group were investigated. Modification of fluorine position exhibited totally different crystalline structures in blending system caused by dissimilar interaction. Furthermore, we have established foundation for the rational designing of π-conjugated molecules with measurement of molecular frontier energy, and light absorption properties.

in chapter 3, I attempted replacement of C-C covalent bond embedded on fused aromatic compounds B←N coordination bond. B←N unit which is isoelectronic and isosteric with C-C unit have exhibited exotic properties in previously reported literatures. In this thesis, I attempted to investigated effects of introducing the B←N unit onto the fused aromatic compounds.

Contents

List of Figures

List of Tables

Introduction.

1. Basic Concepts of Conjugated Molecules.

Most organic polymers have been widely used for insulators or plastics before discovery of π-conjugated polymers. However, discovery of π-conjugated polymer exhibiting electrical conductivity induced by delocalized π-electrons existing along the backbone leads to appear words of *synthetic metals*[1] with mechanical plastic properties and have attracted attention as novel organic materials with exotic properties such as semiconducting properties, light absorbing and emitting properties. Many researchers and scholars have accomplished understanding basic concepts of π-conjugated molecules and utilization for the electronic devices. As a result, π-conjugated molecules have been widely used for the organic photovoltaics (OPVs), field effect transistors (FETs) and light emitting diodes (LEDs). (**Figure 1**).[2]

Figure 1. Diverse applications of π-conjugated molecules for the semiconducting electronic devices.

Among of them, one of the most important thing, revelation of semiconducting properties achieved by π-conjugated system of connected *p*-orbital with delocalized electrons in molecules with alternating single and multiple bonds and these exotic properties (e.g., energy band gap, charge carrier mobility, solid state morphology and mechanical properties) can be tuned successfully through the various modification of molecular structures.[3] Many researchers have studied from modification of π-conjugated molecules to application in various fields and it leads subdivision of fresh research fields into the side chain engineering, modification of backbone, introducing the various functional unit. As a result, present molecular frameworks (**Figure 2**) were invented diversely and further in depth understanding about the fundamentals of the π-conjugated molecules could be accomplished.
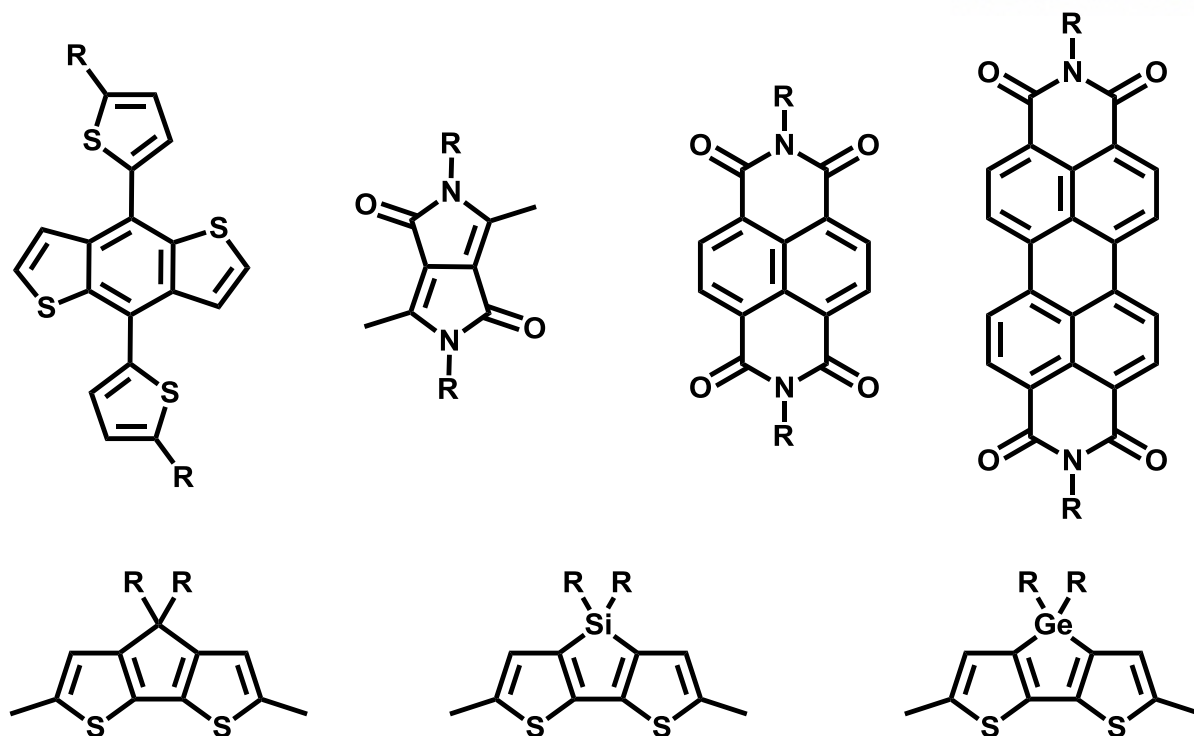
Figure 2. Many kinds of π-conjugated frameworks for the semiconducting materials.

However, despite of many kinds of successful achievements and endeavors, many crucial issues have been remained related with commercialization of π-conjugated molecules. First, π-conjugated molecules have not exhibited comparable performance with devices composed of inorganic materials. Although Jianhui Hou et al. achieved power conversion efficiency (PCE) up to 13.1% in OSC field through the tandem cell architecture,[4] this value stayed below 26.7% PCE based on crystalline cell composed of silicon.[5] Second, π-conjugated polymers occurred variation of properties affecting the performance.[6] Despite small molecules which have mono diversity, diverse variations must be occurred for a variety of reasons (e.g., condition of device fabrication, purity and surrounding environment). Last, they exhibited short-term life-time. Most π-conjugated molecules degenerate not only morphology of solid state but also device characteristics after some time.[7]

These crucial issues imply that there are many undisclosed parts for the understanding the fundamentals and further deep studies have to be attained thoroughly.

2. Introducing the Heteroatoms on Fused Aromatic Compounds.

Among of the many kinds of endeavors for the modulating properties of π-conjugated molecules, introducing the hetero atoms such as silicon (Si), germanium (Ge) and fluorine (F) atoms on fused aromatic compounds have been considered as a most effective methodology.

Electronic property

Strong molecular interaction

Negligible steric effect
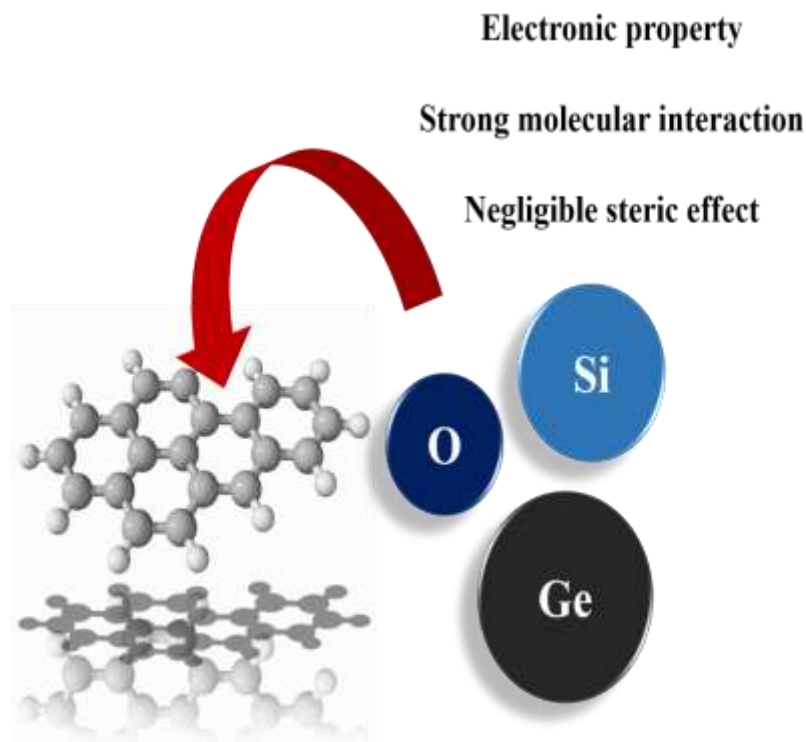
Figure 3. Illustrated basic concepts of introducing the heteroatoms onto the π-conjugated molecules.

Particularly, introducing the heteroatoms on fused aromatic compounds facilitate efficient charge transport with intrinsically high electron affinity. Furthermore, strengthen noncovalent interaction without significant steric effect can modulate morphology of solid state and finally desirable properties are obtained.[8]

Among of previously reported fused heteroaromatic compounds, 7'-(4,4-bis(2-ethylhexyl)-4H-silolo[3,2-b:4,5-b']dithiophene-2,6-diyl)bis(6-fluoro-4-(5'-hexyl-[2,2'-bithio-phen]-5-yl)benzo[c][1,2,5]thiadiazole) (DTSi(FBTTh$_2$)$_2$) designed by Bazan et al.[9] and 7,7'-(4,4-bis(2-ethylhex-yl)-4H-germ-olo[3,2-b:4,5-b']dithiophene-2,6-diyl)bis(6-fluoro-4-(5'-hexyl-[2,2'-bithiophen]-5-yl)-ben-zo[c][1,2,5]thiadiazole) (DTGe(FBTTh$_2$)$_2$) designed by our group are one of the most successful π-conjugated framework with high PCE up to 9% as a single junction device.[10] Especially, strong light harvesting ability within visible ray of these frameworks enough to attract attention and many exotic properties related with these frameworks could be demonstrated.

3. B←N coordination bonding.

Introducing the boron (B) atom and nitrogen atom (N) on the fused aromatic compounds have been studied with many kinds of advantages exhibiting exotic properties diversely.[11]
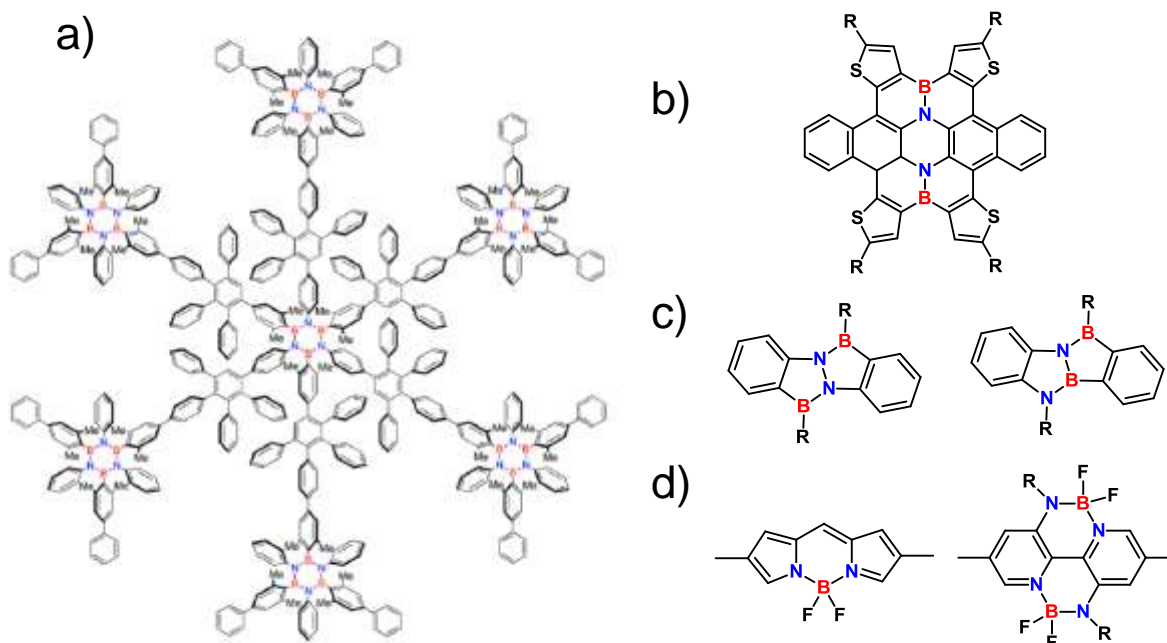
Figure 4. Various B-N doped molecular structures for understanding nature of B-N elements. a) Borazino-doped polyphenylene designed by David Bonifazi et al. and b) BN-embedded dibenzotetrathienocoronene, c) $B_2N_2{}^-$dibenzo[a,e]pentalenes designed by Klaus Müllen et al. and d) typical BODIPY structures.

Among of them, replacement C-C unit covalently linked with B←N unit coordinately linked have been demonstrated as effective modulation to tune the energy level without significant steric effects by Lixiang Wang et al. through the introducing the B←N unit onto the counterpart with isoindigo (IID), dithienyldiketopyrrolopyrrole (DPP), thienopyrrolodione (TPD) units.[12] Furthermore, boron-dipyrrome-thene (BODIPY) has triggered enthusiasm of many researchers for the novel semiconducting materials.[13] However, despite diverse attempts to understand nature of embedding B←N unit onto the heteroaromatic compounds, only few successful examples have been investigated. In this contribution, herein we attempt to study about fundamentals of effect of B←N unit in heteroaromatic π-conjugated molecules.

Chapter Ⅰ. A Comparative Investigation of Cyclohexyl-End-Capped Versus Hexyl-End-Capped Small-Molecule Donors on a Small Donor: Polymer Acceptor Junction Solar Cells

1.1. Abstract.

Replacing hexyl-end-side with cyclohexyl-end-side groups on dithieno[3,2-*b*:2′,3′-*d*]silole (DTSi) and dithieno[3,2-*b*:2′,3′-*d*]germole (DTGe)-based cores yielded two new small-molecule donors: DTSi(FBTTh$_2$Cy)$_2$ and DTGe(FBTTh$_2$Cy)$_2$. Together with the hexyl-end-capped analogs DTSi(FBTTh$_2$)$_2$ and DTGe(FBTTh$_2$)$_2$, the physical properties, morphology, and organic solar cell (OSC) performances with respect to hexyl-end-side versus cyclohexyl-end-side groups were investigated. We observed that the cyclohexyl-end-capped molecules showed blue-shifted film absorptions and lower exothermic crystallization temperatures due to less packed backbones compared to the cyclohexyl-end-capped molecules. When used as donor materials with poly((*N*,*N*′-bis(2-octyldodecyl)-naphthalene-1,4,5,8-bis(dicarboximide)-2,6-diyl)-*alt*-5,5′-(2,2′-bithiophene)) polymer acceptor, the relatively improved open-circuit voltage was achieved from OSCs based on the hexyl-end-capped molecules as a result of their deeper-lying highest occupied molecular orbitals. Nevertheless, the induced higher short-circuit current density and fill factor parameters led to better power conversion efficiencies in the cyclohexyl-end-capped molecule-based OSCs. This was attributed to the preferential face-on orientation with a coarsened morphology, as evidenced by a series of blend film morphological studies. Our experimental findings confirm that the cyclized-end groups in small conjugated materials possess a high potential for improving OSCs.

1.2. Introduction.

Multiple organic semiconductors, including organic solar cells (OSCs), field-effect transistors (FETs), and light-emitting diodes, have been developed to improve the device performances.[14-23] In this regard, several efforts have focused on the design and synthesis of new π-conjugated backbones.[23-31] On the contrary, recently, there has been considerable research demonstrating the substantial impact of the side chains on the device performance with regard to organic semiconductors.[32-39] These results have indicated that even a subtle variation of the side chains, such as chain type and length, branching and substitution position, terminally functionalized groups, chirality, and odd–even-numbered carbon numbers, can significantly impact the device performance.[40-45]

Compared to linear alkyl side chains, cyclic side chains correspond to a special class. When introduced into the conjugated polymer backbones, it is generally documented that the bulkiness of cyclic side chains precludes inter-chain interdigitation, indicating a negative effect on the key parameters of the aforementioned devices.[46] However, several examples with different scenarios have previously been reported. (i) Yang et al. reported that in a given polymer backbone, the cyclic side chains can make the controlling of the polymer self-assembling more effective, which in turn improves the photovoltaic characteristics (e.g., short-circuit current density (J_{SC}), open-circuit voltage (V_{OC}), and fill factor (FF)) using processing additives.[47] (ii) In other reported polymer systems, Facchetti and Marks et al. demonstrated that using cyclic side chains effectively reduces steric hindrance when these cyclic side chains are formed by connecting sp3-hybridized bridgehead silicon atoms, resulting in an enhancement in the charge-transport capacity in FETs.[48] (iii) Bao et al. reported that the cyclohexyl groups add steric bulkiness at the periphery of the molecule that provides improved solubility without having a detrimental effect on the molecular packing in the thin-film phase.[49]

We aim to further understand the impact of cyclic side chains versus acyclic side chains not only on device performance but also on the film microstructure. Therefore, we designed and synthesized two

6

small-molecule donors with cyclohexyl-end-side groups (7,7′-(4,4-bis(2-ethylhexyl)-4*H*-silolo[3,2-*b*:4,5-*b*′]dithiophene-2,6-diyl)bis(4-(5′-cyclohexyl-[2,2′-bithiophen]-5-yl)-6-fluorobenzo[*c*][1,2,5]thiadiazole) (DTSi(FBTTh$_2$Cy)$_2$) and 7,7′-(4,4-bis(2-ethylhexyl)-4*H*-germolo[3,2-*b*:4,5-*b*′]dithiophene-2,6-diyl)bis(4-(5′-cyclohexyl-[2,2′-bithiophen]-5-yl)-6-fluorobenzo[*c*][1,2,5]thiadiazole) (DTGe(FBTTh$_2$Cy)$_2$)) and hexyl-end-capped analogs (7,7′-(4,4-bis(2-ethylhexyl)-4*H*-silolo[3,2-b:4,5-b′]dithiophene-2,6-diyl)bis(6-fluoro-4-(5′-hexyl-[2,2′-bithio-phen]-5-yl)benzo[*c*][1,2,5]thiadiazole) (DTSi(FBTTh$_2$)$_2$) and 7,7′-(4,4-bis(2-ethylhex-yl)-4*H*-germolo[3,2-*b*:4,5-*b*′]dithiophene-2,6-diyl)bis(6-fluoro-4-(5′-hexyl-[2,2′-bithiophen]-5-yl)-benzo[*c*][1,2,5]thiadiazole) (DTGe(FBTTh$_2$)$_2$)) for a comparative study. Recently, driven by their promising advantages over fullerene-based ones, there have been intensive research efforts on fullerene-free based OSCs, including polymer donor/polymer acceptor, polymer donor/non-fullerene small acceptor, and small donor/non-fullerene small acceptor.[50-55] However, to the best of our knowledge, there is only one report related to the small donor/polymer acceptor system.[56] thus, it is still in the early stages of understanding its potential as a new OSC technology. Considering abovementioned aspects, herein, we chose small donor/polymer acceptor systems for not only extending the field of fullerene-free based OSCs but also for further understanding the new bulk heterojunction (BHJ) platform. We evaluated the photovoltaic properties of the small-molecule donor/polymer acceptor OSCs using a combination of the small-molecule donors and the poly((*N,N*′-bis(2-octyldodecyl)-naphthalene-1,4,5,8-bis(dicarboximide)-2,6-diyl)-*alt*-5,5′-(2,2′-bithiophene)) polymer acceptor, known as Activink N2200. We found that compared to the hexyl-end-capped molecule-based OSCs, the cyclohexyl-end-capped molecule-based OSCs provided better performance with improved J_{SC} and FF despite a lower V_{OC} value, which can be attributed to the preferential face-on orientation with a coarsened morphology.

1.3. Results and Discussion.

1.3.1. Synthesis and Characterization.
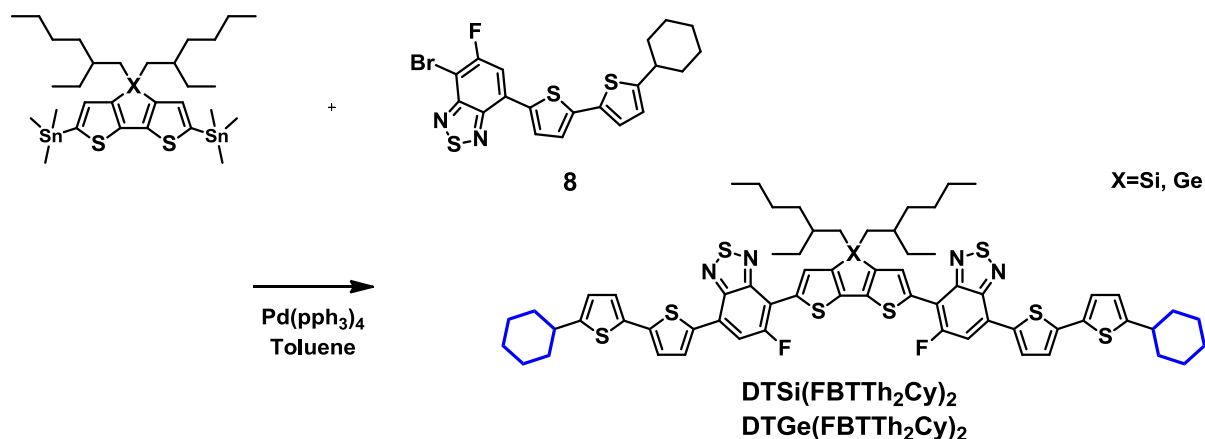
Figure 5. Schematic synthetic pathways for the DTSi(FBTTh$_2$Cy)$_2$ and DTGe(FBTTh$_2$Cy)$_2$.
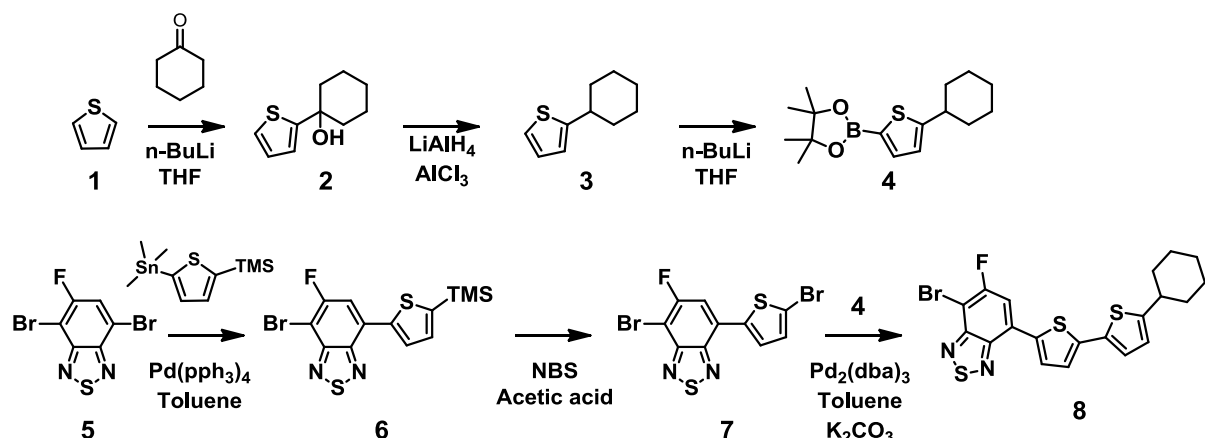
Figure 6. Synthetic steps for the key intermediate.

DTSi(FBTTh$_2$Cy)$_2$ and DTGe(FBTTh$_2$Cy)$_2$ were synthesized in seven steps, as shown in Figure 6. First, 2-cyclohexylthiophene (**3**) was synthesized through the nucleophilic addition of 2-lithiated thiophene to cyclohexanone, followed by reduction with LiAlH$_4$–AlCl$_3$ mixtur-es in 88% overall yield. Then, treatment of **3** with *n*-BuLi and subsequent quenching with 2-isopropoxy-4,4,5,5-tetramethyl-1,3,2-dioxaborolane afforded 2-(5-cyclohexylthiop-hen-2-yl)-4,4,5,5-tetramethyl-1,3,2-dioxaborolane (**4**) in 68% yield. On the contrary, the synthesis of the cyclohexyl-end-capping key intermediate **8** was performed through a combination of a series of cross-coupling reactions and bromination based on the

8

published methods.[56]

Finally, the cyclohexyl-end-capped target oligomers (DTSi(FBTTh$_2$Cy)$_2$ in 44% yield) and (DTGe(FBTTh$_2$Cy)$_2$ in 37% yield) were prepared by microwave-assisted Stille coupling between 8 and the corresponding bis-stannylated aromatic cores (4,4′-bis-(2-ethylhexyl)-dithieno[3,2-*b*:2′,3′-*d*]silole (DTSi) and 4,4′-bis-(2-ethylhexyl)-dithieno[3,2-*b*:2′,3′-*d*]germole (DTGe)), respectively. Both DTSi(FBTTh$_2$Cy)$_2$ and DTGe(FBTTh$_2$Cy)$_2$ exhibited a good solubility in various organic solvents. We confirmed their high purity and molecular structur-es via NMR spectroscopy, mass spectroscopy, and elemental analysis (EA). The detailed syn-thesis and characterization are provided in Experimental Section. For a fair comparison, as mentioned in Introduction, the hexyl-end-capped analogs (DTSi(FBTTh$_2$)$_2$ and DTGe(FBTTh$_2$)$_2$) were also synthesized by the procedure reported in previous research[57] and a comparative discussion will be presented in the following sections.

1.3.2. Optical, Electrochemical, Thermal and Theoretical Characterizations.
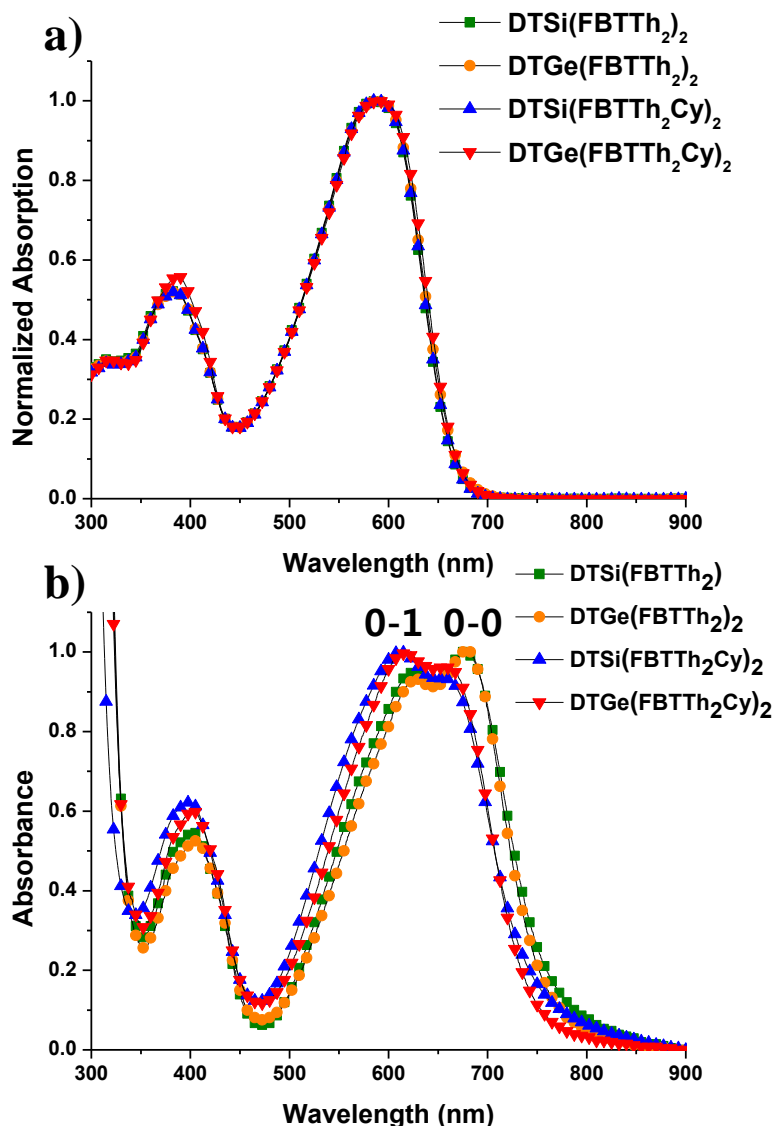
Figure 7. UV-vis spectra of DTSi- and DTGe-based small molecules in (a) chloroform solutions and as (b) thin films.

We measured the UV–Vis absorption spectra of DTSi(FBTTh$_2$Cy)$_2$ and DTGe(FBTTh$_2$Cy)$_2$ in chloroform solutions and thin films (Figure 7) and summarized the relevant data in Table 1. DTSi(FBTTh$_2$Cy)$_2$ and DTGe(FBTTh$_2$Cy)$_2$ in chloroform have considerably similar absorption bands in the range 350–700 nm, with an absorption maximum (λ_{max}) of 590 nm, which are nearly identical to those of hexyl-end-capped analogs (DTSi(FBTTh$_2$)$_2$ and DTGe(FBTTh$_2$)$_2$). In the thin films, the absorption spectra of both the molecules show broader absorption with redshifts compared to the

solution spectra due to the stronger intermolecular interaction on the condensed solid state, as observed in several other conjugated materials. For both cases, a considerably similar optical band gap (E_g^{opt}) of ~1.66 eV was determined by the onsets (λ_{onset}) of their absorption films. Interestingly, clear differences were observed in the absorption film profiles between the cyclohexyl-end-capped and hexyl-end-capped samples. For example, compared to hexyl-end-capped analogs, the λ_{max} and λ_{onset} values of $DTSi(FBTTh_2Cy)_2$ and $DTGe(FBTTh_2Cy)_2$ films were blueshifted and the 0–1 vibrational transitions relative to 0–0 ones were intensified. These results indicate that the structural change of the alkyl side chain from hexyl to cyclohexyl groups leads to longer inter-chain distances, thereby reducing the backbone inter-chain interaction. Similar behaviors were also reported for π-conjugated polymers appended with these cyclic side chains due to intra- or inter-molecular steric hindrance effects.[58-59]

Table 1. Optical and electrochemical properties of the DTSi- and DTGe-based small molecules. The HOMO (eV) = − ($E_{(ox)}^{onset}$ − $E_{(ferrocene)}^{onset}$ + 4.8) and LUMO (eV) = − ($E_{(red)}^{onset}$ − $E_{(ferrocene)}^{onset}$ + 4.8) were calculated from CV results.

Compound	Solution		Film			CV	
	λ_{max} [nm]	λ_{onset} [nm]	λ_{max} [nm]	λ_{onset} [nm]	E_g [eV]	HOMO [eV]	LUMO [eV]
$DTSi(FBTTh_2)_2$	588	689	677	762	1.63	-5.13	-3.37
$DTGe(FBTTh_2)_2$	592	686	677	760	1.63	-5.14	-3.38
$DTSi(FBTTh_2Cy)_2$	588	671	612	751	1.65	-5.05	-3.26
$DTGe(FBTTh_2Cy)_2$	591	670	616	748	1.66	-5.08	-3.25

The frontier energy levels (the highest occupied molecular orbital (HOMO) and the lowest unoccupied molecular orbital (LUMO)) of these molecules have been investigated via cyclic voltammetry in a liquid electrolyte. The onset oxidation and reduction potentials (E_{ox}^{onset}/E_{red}^{onset}) of $DTSi(FBTTh_2Cy)_2$ and $DTGe(FBTTh_2Cy)$ were measured to be −0.29/1.58 V and −0.32/1.59 vs. Ag/Ag+ and their HOMO energy level (E_{HOMO})/LUMO energy level (E_{LUMO}), which were calculated to be −5.05/−3.26 eV and −5.08/−3.25 eV, respectively, according to the following equations: HOMO (eV) = − ($E_{(ox)}^{onset}$ − $E_{(ferrocene)}^{onset}$ + 4.8) and LUMO (eV) = − ($E_{(red)}^{onset}$ − $E_{(ferrocene)}^{onset}$ + 4.8), where the ferrocene/ferrocenium (Fc/Fc+) redox couple with a standard energy level of −4.8 eV appeared at 0.04 V. In addition, the HOMO/LUMO values of the hexyl-end-capped samples were found to be −5.13/3.37 and −5.14/3.38 for $DTSi(FBTTh_2)_2$ and $DTGe(FBTTh_2)$, respectively, under the same condition. All the relevant data are summarized in Table 1. It is worth noting that the hexyl-end-

capped samples have slightly deeper-lying HOMO and LUMO levels compared to those of the corresponding cyclohexyl-end-capped analogs, which are beneficial for enhancing the open-circuit voltage V_{OC} of the OSCs based on the compounds as donor. This trend is opposite to what was previously observed in π-conjugated polymers appended with cyclic side chains.[58-60]
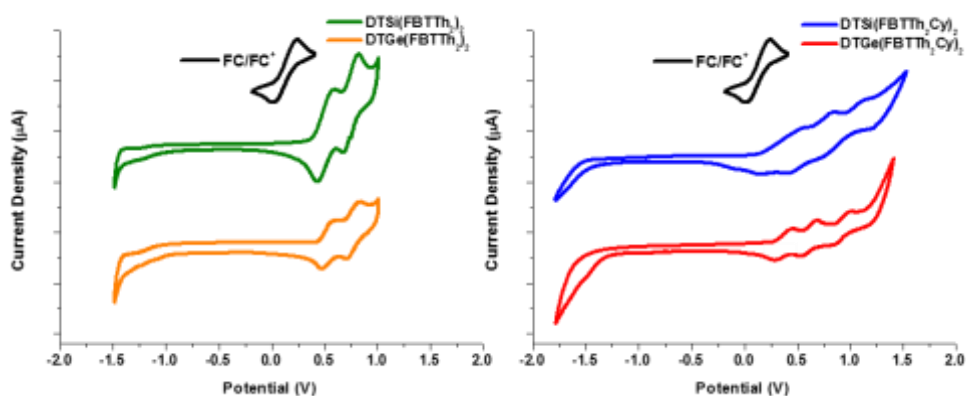
Figure 8. Cyclic voltammograms of DTSi- and DTGe-based small molecules in n-Bu$_4$NPF$_6$/CHCl$_3$ solutions with Fc/Fc+ as external reference (scan rate : 100 mV/s).
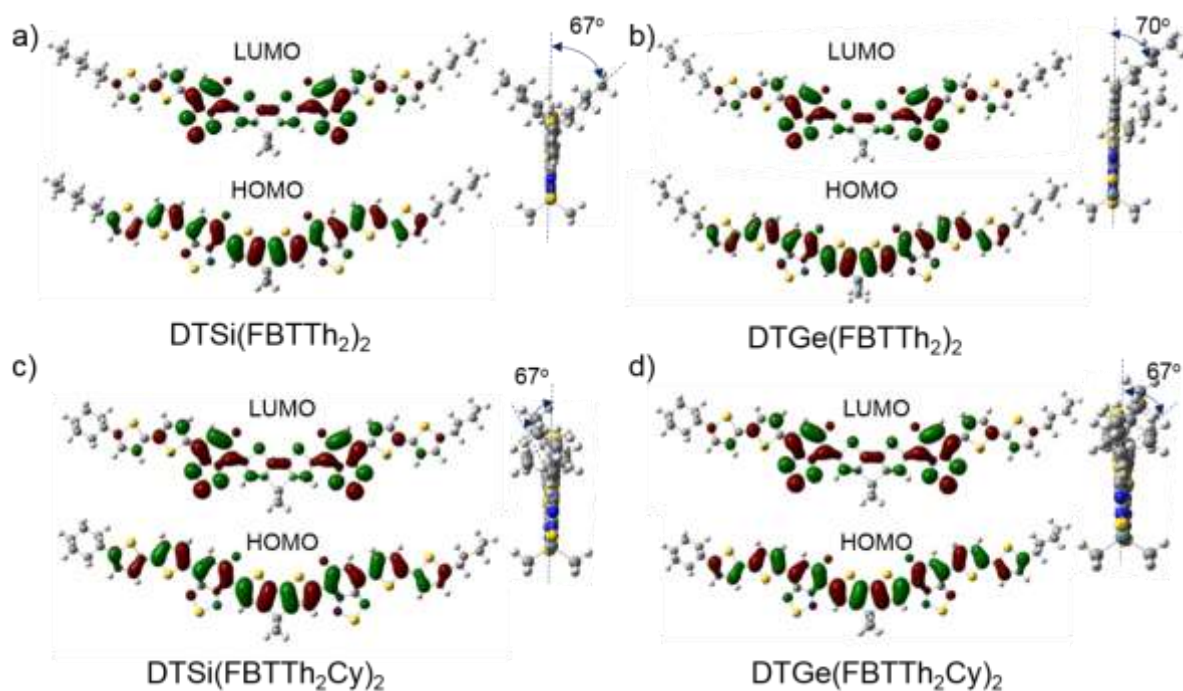
Figure 9. Molecular conformation and frontier orbital geometries for a) DTSi(FBTTh$_2$), b) DTGe(FBTTh$_2$)$_2$, c) DTSi(FBTTh$_2$Cy)$_2$ and d) DTGe(FBTTh$_2$Cy)$_2$ calculated by DFT.

We also performed theoretical calculations on the molecular geometries and electronic wave functions of frontier orbitals using the density functional theory (DFT) method under B3LYP and a 6-31G basis set. As shown in Figure 4, for all these molecules, the molecular backbones exhibit similar geometries, e.g., high co-planarity of conjugated backbone and similar electron density distributions of the HOMO and LUMO orbitals. In addition, there is nearly no difference in the twist angle between the end-side chains and the plane of the backbone ($\theta_1 \approx 67°-70°$). Additionally, note that the calculated HOMO/LUMO trends were well correlated with the above CV results.
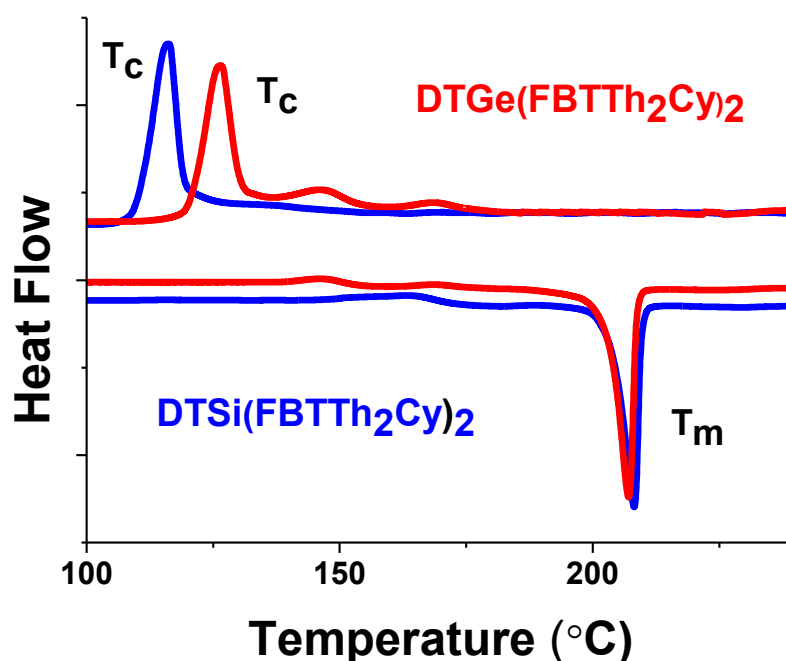
Figure 10. DSC curves for DTSi(FBTTh$_2$Cy)$_2$ and DTGe(FBTTh$_2$Cy)$_2$.

The differential scanning calorimetry (DSC) heating curves of both DTSi(FBTTh$_2$Cy)$_2$ and DTGe(FBTTh$_2$Cy)$_2$ showed a distinct endothermic melting peak (T_m) with a similar temperature of ~208 °C, while their exothermic crystallization (T_c) occurs at different temperatures (116 °C for DTSi(FBTTh$_2$Cy)$_2$ and 127 °C for DTGe(FBTTh$_2$Cy)$_2$) during the cooling cycle (Figure 10). In addition, note that the reason for the presence of additional small peaks in the DSC of DTGe(FBTTh$_2$Cy)$_2$ is unclear; however, this could be due to the result of an intermediate phase. The T_m/T_c values of the hexyl-end-capped analogs have been already reported (209 °C/173 °C, DTSi(FBTTh$_2$)$_2$ and 203 °C/167 °C, (DTGe(FBTTh$_2$)$_2$).[61] Based on these comparison data, we can suggest that varying the terminal chains from hexyl to cyclohexyl groups leads to a kinetical change in the crystallization process but has little impact on the melting processing.

1.3.5. Device Fabrication and Thin Film Morphology.

BHJ OSCs were fabricated with DTSi- and DTGe-based small-molecule donors and N2200 polymer acceptor using a conventional solution spin-coating process. The detailed fabrication procedure is described in Experimental Section. The device structure is indium-tin oxide (ITO)/poly(3,4-ethylenedioxythiophene):poly(styrenesulfonate) (PEDOT:PSS)/active layer/Al. Photovoltaic performance measurements were performed under an illumination of AM 1.5G simulated solar light at 100 mW cm^{-2}. Device optimization was conducted at the optimized donor/acceptor ratio (3:2 w/w) in a chlorobenzene solution containing 0.2 vol% 1,8-diiodooctane (DIO) additive. Thermal annealing was performed at various temperatures for each 10 min in an inert atmosphere since we observed different isothermal crystallization behaviors depending on the end-side chains.
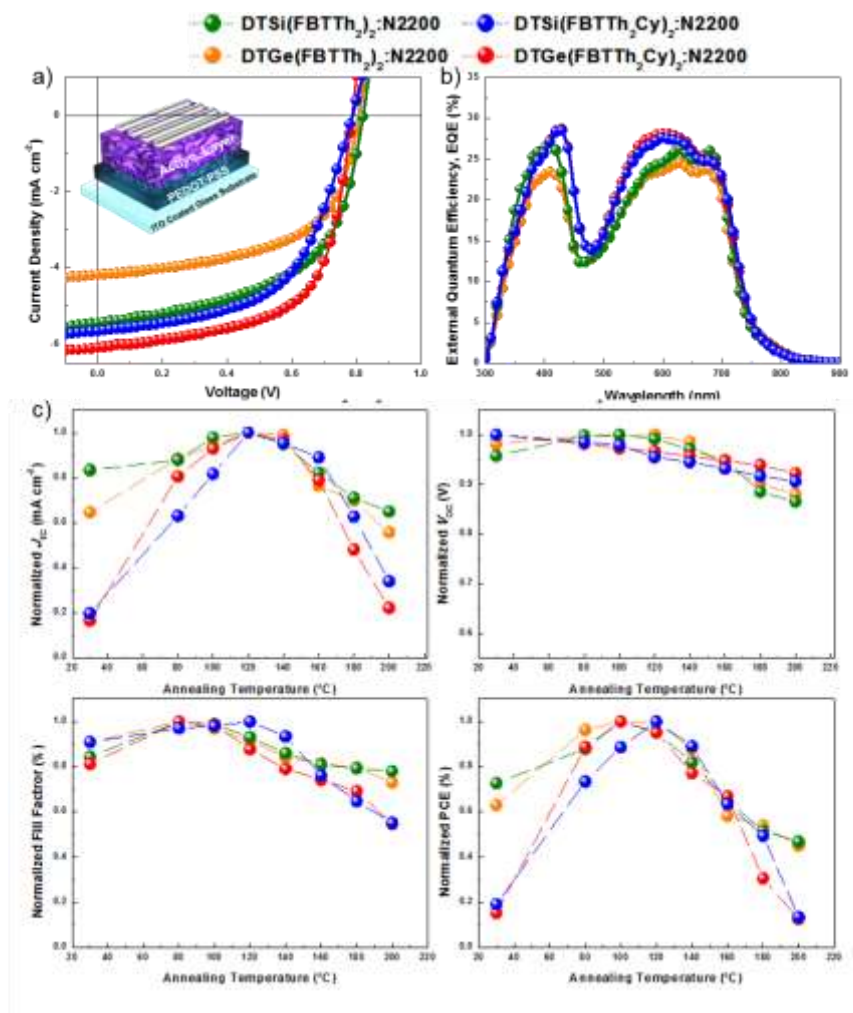
Figure 11. *J–V* curves (ITO/PEDOT:PSS/active layer/Al) (a) and EQE spectra (b) of the optimized devices. Dependence of the photovoltaic parameters on different annealing temperatures (c).

14

Among the devices based on these four donors, the DTGe(FBTTh$_2$Cy)$_2$:N2200 system showed the best PCE (3.04%) with the highest J_{SC} value (6.08 mW cm^{-2}), the highest FF value (63%), and a moderate V_{OC} value (0.78 V). As shown in Figure 5c, the observed variations in the J_{SC} values with different copolymer compositions were well reflected in the changes of their spectral response in the external quantum efficiency (EQE) spectra. Additionally, Figure 5 shows the annealing temperature dependence of the photovoltaic performance, including the J_{SC}, V_{OC}, FF, and PCE values. For evaluated temperatures over 120 °C, all devices were subject to a significant decrease in all photovoltaic parameters, particularly J_{SC} values.

We can reasonably speculate that all the small molecules have temperature-dependent aggregation behavior, leading to a significant change in the blend morphology with high temperatures (>120 °C).

Table 2. Optimized device parameters of OSCs based on DTSi- and DTGe-small molecules under100 mW cm^{-2} AM 1.5G solar illumination.*

Active layer	J_{sc} [mW cm^{-2}]	V_{OC} [V]	FF [%]	PCE [%]
DTSi(FBTTh$_2$)$_2$:N2200	5.40 (5.51)	0.823(0.825)	55.2(56.4)	2.30(2.45)
DTGe(FBTTh$_2$)$_2$:N2200	4.16(4.18)	0.806(0.807)	57.2(57.7)	1.91(1.95)
DTSi(FBTTh$_2$Cy)$_2$:N2200	5.52(5.65)	0.783(0.784)	59.0(60.0)	2.41(2.68)
DTGe(FBTTh$_2$Cy)$_2$:N2200	5.74(6.08)	0.784(0.787)	62.6(63.3)	2.77(3.04)

*The photovoltaic properties were averaged over eight devices and the maximum values were given in parentheses.

The structural order and crystallinity of the four donor materials in the optimized blend films were studied via grazing-incidence wide-angle X-ray scattering (GIWAXS). As evident in Figures 6a and 6b, both the hexyl-end-capped molecule-based blend films exhibited highly ordered (h00) diffraction peaks (up to third order; d ~ 24 Å) along the out-of-plane (q_z) direction with the (010) π–π diffraction peak (d ~ 3.6 Å) in both in-plane (q_{xy}) and q_z profiles, suggesting the long-range ordered lamellar structure with a mixed edge-on and face-on orientation relative to the substrate. On the contrary, the cyclohexyl-end-capped molecule-based blend films exhibited similar (100) and (200) diffraction peaks, whereas the (010) π–π diffraction peak along only q_z, implying that the face-on orientation with respect to the substrate is the preferred orientation for these blends.

15

In addition, we obtained the area ratio of A_{XY} to A_Z (A_{XY}/A_Z) using pole figures along the (100) lamellar diffraction peaks (Figure 6). The ratio values were in the order of $DTGe(FBTTh_2Cy)_2$ (0.83) > $DTSi(FBTTh_2Cy)_2$ (0.73) > $DTSi(FBTTh_2)_2$ (0.19) > $DTGe(FBTTh_2)_2$ (0.17), supporting a more pronounced tendency to face-on orientation in the cyclohexyl-end-capped molecule-based blends.
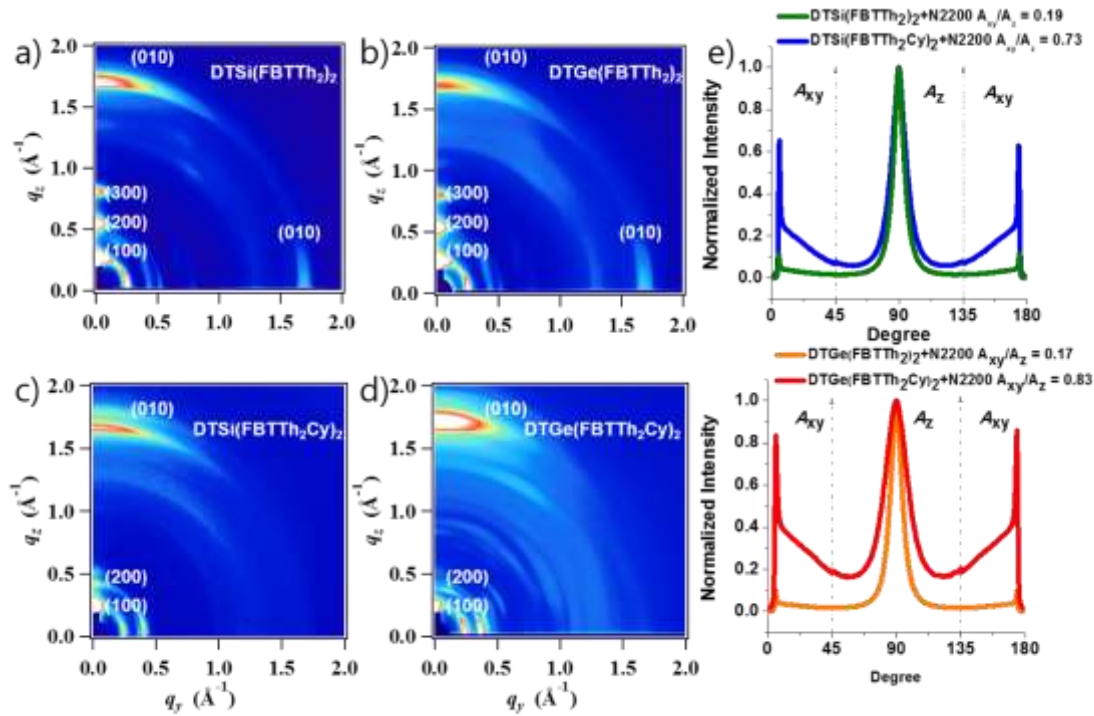
Figure 12. GIWAXS images (a-d) of the optimized blending films and their pole figure plots (e) obtained from the (100) lamellar diffraction; the integrated areas of A_{xy} (0°−45° and 135°−180°) and A_z (45°−135°) indicate the preferable orientations.

On the contrary, slightly shorter lamellar distances ($d \sim 22$ Å) were observed from hexyl-end-capped molecule-based blends. This finding well agrees with the overall experimental data, as discussed above. It is well known that the face-on orientation is more favorable for photovoltaic devices because of its vertical charge transportation channel. Therefore, we speculate that the formation of the preferential face-on orientation in the blends is a more significant effect on the overall performance than the tightly packed structure.

16
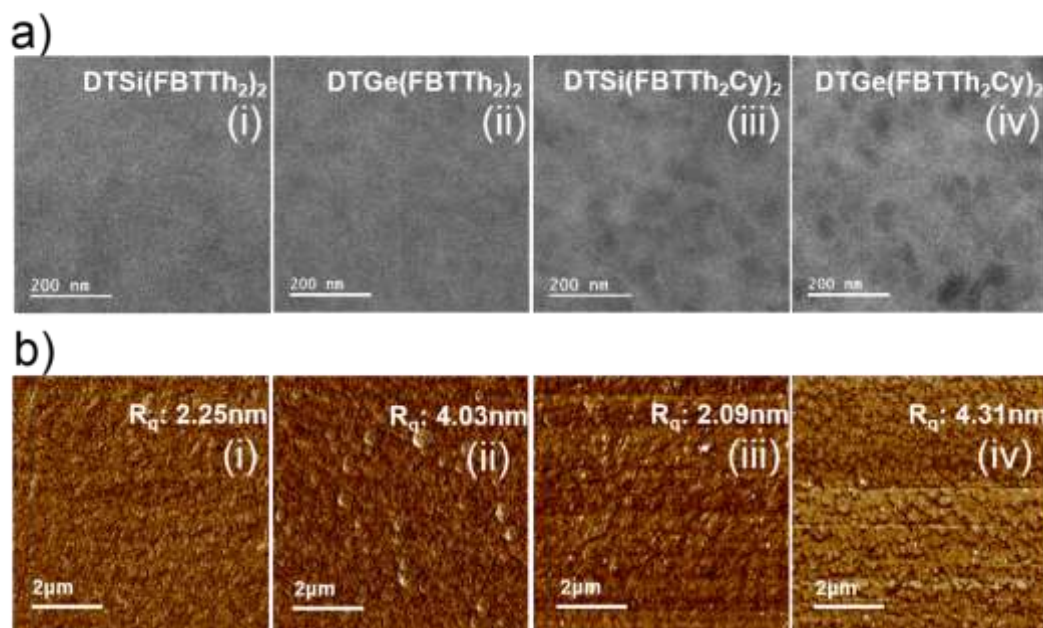
Figure 13. AFM height (a) and TEM (b) images of optimized blend films.

We also investigated the surface and bulk morphologies of the optimized blend films using tapping-mode atomic force microscopy (AFM) and transmission electron microscopy (TEM). The AFM images shown in Figure 7 reveal that the hexyl-end-capped molecule-based blend films have a relatively smooth surface with a root-mean-square (RMS) roughness of 2.25 nm for the DTSi(FBTTh$_2$)$_2$/N2200 film and 2.09 nm for the DTGe(FBTTh$_2$)$_2$/N2200 blend film, while relatively coarse surfaces with a RMS roughness range of 4.03–4.31 nm were observed in the cyclohexyl-end-capped molecule-based blend films. In addition, the TEM images reveal that a homogeneous morphology with inconspicuous phase separation features was found for hexyl-end-capped molecule-based blend films, whereas slightly coarsened domains were observed in the cyclohexyl-end-capped molecule blend films. The AFM and TEM data suggest that the hexyl-end-capped molecules can provide somewhat better miscibility with the N2200 polymer in the blend films.

Furthermore, to investigate effect of incorporation of cyclo chain, we have studied about blending system with [6,6]-phenyl-C71-butyric acid methyl ester (PC$_{71}$BM) as an acceptor additionally. In this system, thermal annealing experiments were also progressed for the subtle morphological changes and normalized device characteristics are shown in **Figure 19**. Although dramatic decay of J_{sc} were exhibited during the thermal annealing in this system, PCE was improved through the enhanced open circuit voltage (V_{oc}) except for the DTSi(FBTTh$_2$Cy)$_2$.
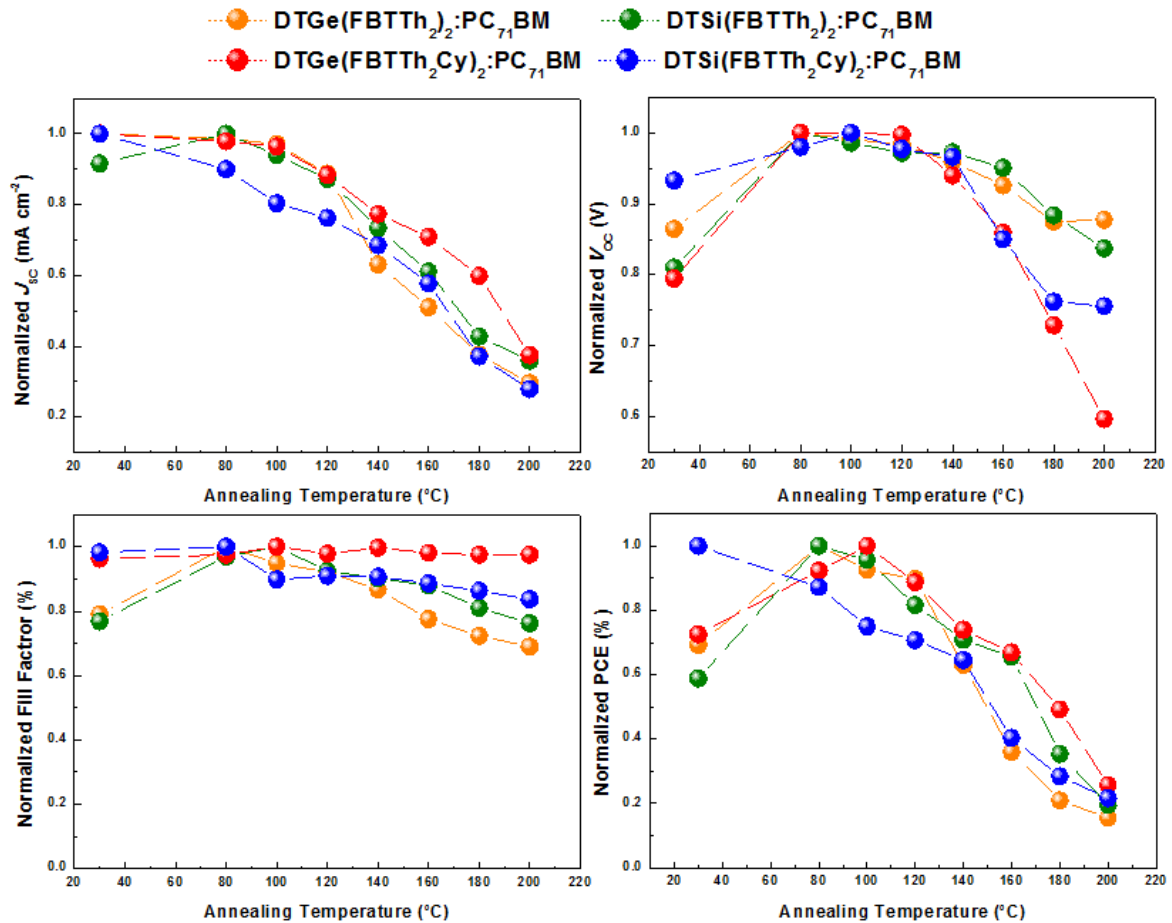
Figure 14. Normalized device parameters depend on different annealing temperatures with PC$_{71}$BM.

18

And optimized EQE, *J-V* curves and device parameters shown in **Figure 20** and **Table 3** respectively
after thermal annealing.
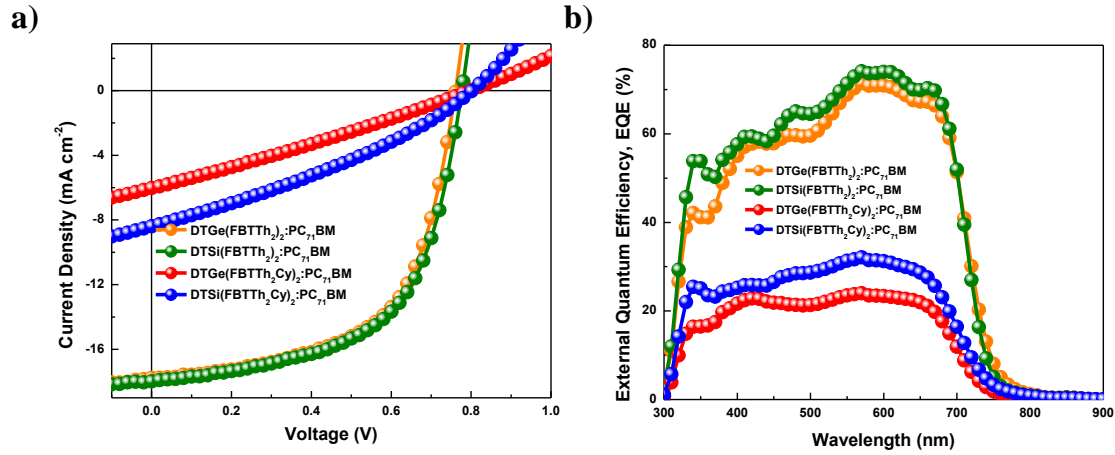
Figure 15. *J-V* curves (a) and external quantum efficiency (b) of optimized blending films with $PC_{71}BM$.

Table 3. Optimized device parameters under 100 mW cm^{-2} AM 1.5G solar illumination with $PC_{71}BM$.

Samples	J_{sc}	V_{OC}	FF	Eff
	[mA cm^{-2}]	[V]	[%]	[%]
DTSi(FBTTh$_2$Cy)$_2$: PC$_{71}$BM	8.12 (8.38)	0.779 (0.802)	0.318 (0.322)	2.16 (2.10)
DTGe(FBTTh$_2$Cy)$_2$: PC$_{71}$BM	6.35 (6.52)	0.776 (0.780)	0.288 (0.290)	1.43 (1.46)
DTSi(FBTTh$_2$)$_2$: PC$_{71}$BM	17.40 (18.00)	0.776 (0.779)	0.561 (0.597)	7.89 (8.34)
DTGe(FBTTh$_2$)$_2$: PC$_{71}$BM	17.00 (17.80)	0.778 (0.780)	0.584 (0.610)	7.76 (8.29)

Especially, both compounds of DTSi(FBTTh$_2$)$_2$ and DTGe(FBTTh$_2$)$_2$ exhibited higher PCE at 8.34%
and 8.29% with higher J_{sc} and FF compared to the DTSi(FBTTh$_2$Cy) and DTGe(FBTTh$_2$Cy)$_2$
respectively. These results indicated that incorporation of cyclo chain affect unfavorable miscibility
with $PC_{71}BM$ rather than forming the fine- tuned morphology and it will be discussed below with
GIWAXS images, AFM and TEM images.

GIWAXS images of all optimized blending films with $PC_{71}BM$ are illustrated in **Figure 21**. As noted from images, both compounds of $DTSi(FBTTh_2Cy)_2$ and $DTGe(FBTTh_2Cy)_2$ does not exhibited any arcs patterns except for the patterns of faint (100) peak and $PC_{71}BM$ and it inferred amorphous orientation of blending system. On the other hand, $DTSi(FBTTh_2)_2$ and $DTGe(FBTTh_2)_2$ exhibited distinct arcs patterns and longer-range ordered (h00) along the both planes of in-plane and out-of-plane directions corresponding line cuts results (**Figure 22**).
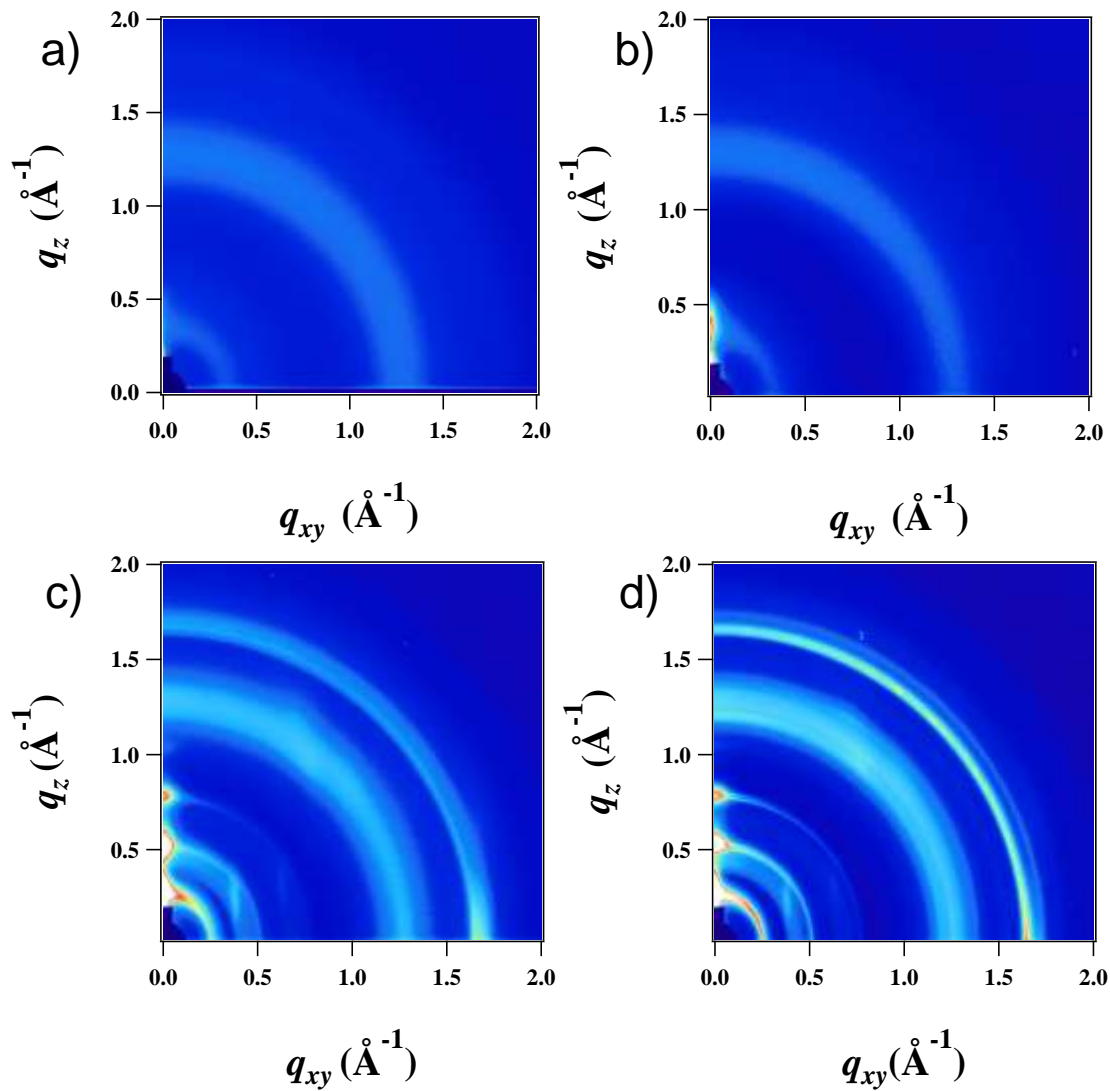
Figure 16. 2D-GIWAXS images of optimized blending films with $PC_{71}BM$ thermal annealed $DTSi(FBTTh_2Cy)_2$ (a), $DTGe(FBTTh_2Cy)_2$ (b), $DTSi(FBTTh_2)_2$ (c), $DTGe(FBTTh_2)_2$ (d).

20
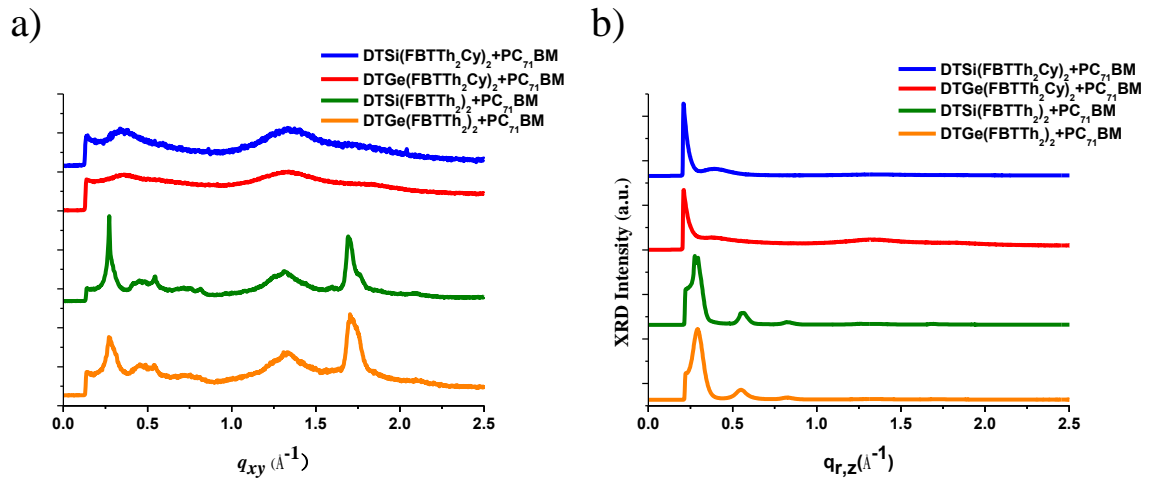
Figure 17. Line cuts of optimized blending films with $PC_{71}BM$ along the in-plane (a) and out-of-plane (b).

These results indicated that both compounds of $DTSi(FBTTh_2)_2$ and $DTGe(FBTTh_2)_2$ achieved well-defined morphology with $PC_{71}BM$ and it leads higher PCE with enhanced J_{sc} and FF attributed to ideal microstructures related with charge transporting ability. These ideal morphologies in surface and bulk state were also observed on AFM and TEM images (**Figure 23**).
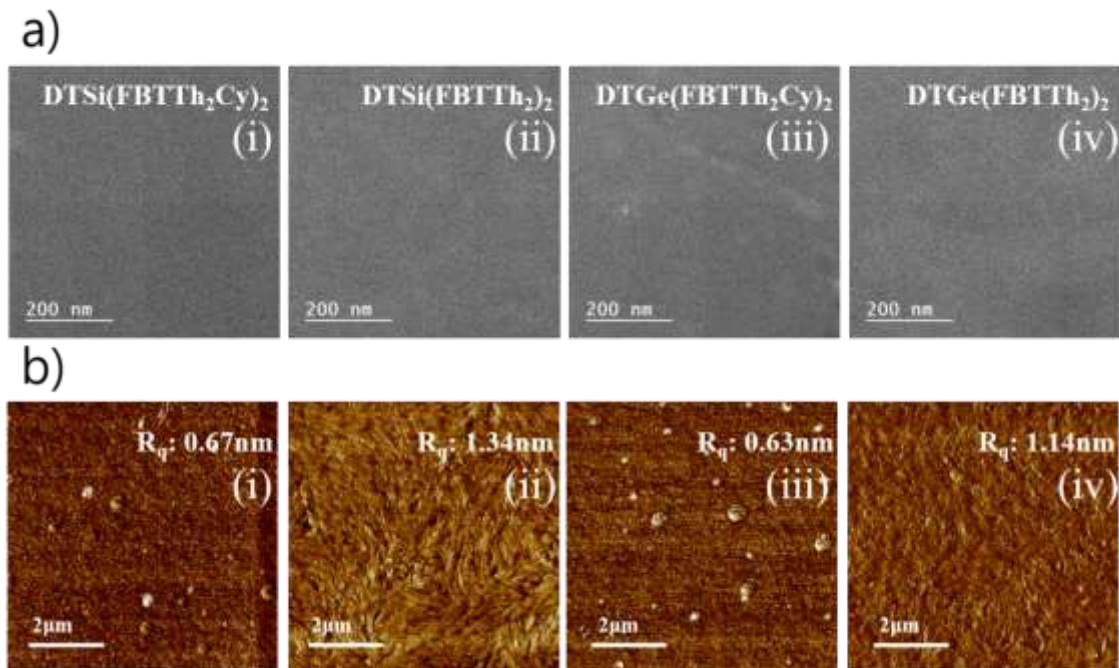
Figure 18. a) TEM and b) AFM images of optimized blend films with $PC_{71}BM$.

Blended films of $DTSi(FBTTh_2)_2$ and $DTGe(FBTTh_2)_2$ with $PC_{71}BM$ exhibited 1.34, 1.14 nm R_q value indicating surface roughness and $DTSi(FBTTh_2Cy)_2$ and $DTGe(FBTTh_2Cy)_2$ exhibited 0.67,

21

0.63 nm respectively. Especially, AFM images of DTSi(FBTTh$_2$)$_2$ and DTGe(FBTTh$_2$)$_2$ recorded distinct fibril-like structures indicating that donor could intercalate onto the acceptor phase well and it facilitated advanced charge dissociation of exciton induced by incidence of photon on the interface between donor and acceptor. On the other hand, aggregated particles which could not be mixed were recorded in AFM images of DTSi(FBTTh$_2$Cy)$_2$ and DTGe(FBTTh$_2$Cy)$_2$. These results mean that incorporation of cyclic chain make repulsion with PC$_{71}$BM different from N2200 blending system and non-cylic chain leads effective packing orientation with PC$_{71}$BM arousing significant improvements of device performance.

1.4. Conclusion.

In summary, two new DTSi(FBTTh$_2$Cy)$_2$ and DTGe(FBTTh$_2$Cy)$_2$ with cyclohexyl-end side chains were synthesized and characterized. A comparative study of the two resulting molecules and the hexyl-end-capped analogs (DTSi(FBTTh$_2$)$_2$ and DTGe(FBTTh$_2$)$_2$) allowed us to identify the design principles that can be applied to influence the optical and electrochemical properties, film morphology, and OSC performance. Compared with the hexyl-end-capped analogs, the cyclohexyl-end-capped molecules exhibited slightly blue shift of the film absorption and lower T$_c$ value due to the reduced backbone intra-/inter-molecular interactions.

Unexpectedly, the hexyl-end-capped analogs had deeper-lying HOMO and LUMO levels, which led to the improvement of V_{OC} when blended with the N2200 polymer acceptor. The morphologies of the cyclohexyl-end-capped molecule/N2200 blend films revealed a more pronounced face-on character with a coarsened feature, whereas the hexyl-end-capped analog/N2200 blend films had a more ordered and shorter lamellar structure with homogeneity. Such microstructural differences contributed to the relatively enhanced PCEs with higher J_{SC} and FF values in cyclohexyl-end-capped molecule-based OSCs compared to the hexyl-end-capped molecule-based counterparts. Our results demonstrate that replacing the linear-end side chains with the corresponding cyclized end groups can influence the molecular orientation of the blend films and potentially result in a positive effect for achieving higher performance of OSCs.

1.5. Experimental Section.

Materials and Instruments: All the chemicals and reagents were purchased from Sigma Aldrich, Alfa Aesar Chemical Company, and Solarmer and used without further purification. All solvents are ACS and anhydrous grade by distillation. All the intermediates (1–7),[56-57, 62] $DTSi(FBTTh_2)_2$, and $DTGe(FBTTh_2)_2$ were synthesized by previously reported literatures. ^{1}H NMR and ^{13}C NMR spectra were recorded on an Agilent 400 MHz spectrometer using deuterated $CDCl_3$ as solvent and tetramethylsilane (TMS) as an internal standard. Elementary analyses were carried out with a Flash 2000 element analyzer (Thermo Scientific, Netherlands) and MALDI-TOF MS spectra were checked by Ultraflex III (Bruker, Germany). UV-Vis absorption spectra in solution and in thin films were measured on a UV-1800 (SHIMADZU) spectrophotometer. Cyclic voltammetry (CV) measurements were performed on AMETEK Versa STAT 3 with a three-electrode cell system in a nitrogen bubbled 0.1 M tetra-n-butylammonium hexafluorophosphate (n-Bu_4NPF_6) solution in chloroform at a scan rate of 100 mV/s at room temperature. Ag/Ag^+ electrode, platinum wire, and carbon glassy were used as the reference electrode, counter electrode, and working electrode, respectively. The Ag/Ag^+ reference electrode was calibrated using a ferrocene/ferrocenium redox couple as an external standard, whose oxidation potential is set at -4.8 eV with respect to a zero-vacuum level. The HOMO energy levels were obtained from the equation HOMO (eV) = $- (E_{(ox)}^{onset} - E_{(ferrocene)}^{onset} + 4.8)$. The LUMO levels were obtained from the equation LUMO (eV) = $-(E_{(red)}^{onset} - E_{(ferrocene)}^{onset} + 4.8)$. DFT calculations were performed using the Gaussian 09 package with the nonlocal hybrid Becke three-parameter Lee-Yang-Parr (B3LYP) function and the 6-31G basis set to elucidate the HOMO and LUMO levels after optimizing the geometry of small molecules using the same method.

Device fabrication: The ITO coated glass substrates (15 Ω^{-1}) were sequentially cleaned by ultra-sonicating in liquid detergent, deionized water, acetone and isopropanol for 15 minutes each. The washed ITOs were dried in oven at 70 °C for overnight. For preparation of N2200 based different ratios of D/A (3:1, 3:1.5, 3:2, and 3:3 w/w) with donor concentration of 24mg/ml in chlorobenzene were used to optimize the active layer morphology. The solution was heated at 30 °C for overnight under minimal stirring. Thereafter, the heating temperature was raised to 60 °C and 0.2 vol% of DIO was added and stirred for another 3 hours. Prior to device fabrication, cleaned ITOs were treated with UV-Ozone treatment for 30 minutes and then a thin PEDOT:PSS (Baytron P VP AI 4083, H. C. Starck) layer was deposited over ITO surface at 4000 rpm. After sequentially annealed at 140 °C for 20 minutes, the substrates were transferred to the nitrogen filled glove box. 30 µl of the active layer solution was added on PEDOT:PSS coated ITOs through dynamic dispense at 4500 rpm in active layer solution for 40 seconds. The films were dried for 10 minutes in petri dish and then dried in vacuum chamber for 30

minutes to remove extra solvents. 100 nm Al cathode was thereafter thermally evaporated on top of the organic layer using the mask (device area: 0.13 cm^2) under the pressure of $< 9\times10^{-7}$ torr. The devices were annealed at different annealing temperatures for 10 minutes prior to the measurement as discussed above.

Synthesis of 4-bromo-7-(5'-cyclohexyl-[2,2'-bithiophen]-5-yl)-5-fluorobenzo[c][1,2,5]thia-diazole **8**: The toluene (20 mL) solution of 4-bromo-7-(5-bromothiophen-2-yl)-5-fluorobenzo[c][1,2,5]thiadiazole (1.5 g, 3.83 mmol) and 2-(5-cyclohexylthiophen-2-yl)-4,4,5,5-tetramethyl-1,3,2-dioxaborolane (1.23 g, 4.21 mmol) was charged in long Schlenk flask under argon. After that, Pd$_2$(dba)$_3$ (87.98 mg, 0.096 mmol), tri(o-tolyl)phosphine (87.65 mg, 0.288 mmol) and K$_2$CO$_3$ (2.65 g, 19.15 mmol) were added into the reaction flask. The reaction mixture was stirred for 3 days at 110 °C. After cooling, the crude organic compounds were extracted with ether at three times, and then the solvent was evaporated. The product was purified by flash column chromatography using a hexanes/chloroform as an orange solid. Yield: 1.28 g (71%). ^{1}H NMR (400 MHz, CDCl$_3$) δ 8.02 (d, J = 4.0 Hz, 1H), 7.64 (d, J = 12.0 Hz, 1H), 7.16 (dd, J = 4.0, 12.0 Hz, 1H), 7.12 (d, J = 4.0 Hz, 1H), 6.74 (d, J = 4.0 Hz, 1H), 2.81 (m, 1H), 2.14 – 2.03 (m, 2H), 1.95 – 1.78 (m, 2H), 1.43 (m, 4H), 1.34 – 1.14 (m, 2H). ^{13}C NMR (100 MHz, CDCl$_3$) δ 154.23, 153.16, 148.88, 141.25, 135.02, 134.99, 133.45, 129.90, 127.38, 124.19, 123.83, 122.98, 115.47, 115.17, 39.68, 35.30, 33.60, 30.95, 26.40, 25.90. Elemental Analysis Calc. for C$_{20}$H$_{16}$BrFNS$_3$: C 50.10, H 3.36, N 5.84, S 20.26; Found: C 50.23, H 3.38, N 5.92, S 20.42. Electron Ionization (EI) MS: Calcd. for 479.45; Found 480.25.

Synthesis of DTSi(FBTTh$_2$Cy)$_2$: A microwave-assisted Stille coupling between 4,4-bis(2-ethylhexyl)-2,6-bis(trimethylstannyl)-4H-silolo[3,2-b:4,5-b']dithiophene (400 mg, 0.54 mmol) and **8** (541 mg, 1.13 mmol) was carried out by using the previous our synthetic condition.[45] The product was purified by flash chromatography using a hexanes/chloroform as a deep blue solid. Yield: 286 mg (44%). ^{1}H NMR (400 MHz, CDCl$_3$) δ 8.27 (s, 2H), 7.88 (s, 2H), 7.51 (d, J = 12.0Hz, 2H), 7.04 (dd, J = 4.0, 12.0 Hz, 4H), 6.67 (d, J = 4.0 Hz, 2H), 2.76 (br s, 2H), 2.05 – 1.55(m, 12H), 1.45 – 1.20 (m, 30H), 0.87 (m, 12H). ^{13}C NMR (100 MHz, CDCl$_3$) δ 159.77, 155.77, 153.93, 152.71, 149.42, 145.14, 144.10, 138.27, 136.26, 133.78, 129.35, 126.88, 125.36, 123.67, 122.77, 122.54, 103.05, 102.80, 40.18, 39.59, 36.10, 35.88, 35.26, 30.95, 29.13, 28.97, 26.42, 25.93, 23.13, 17.86, 14.27, 10.89. Elemental Analysis Calc. for C$_{64}$H$_{68}$F$_2$N$_4$S$_8$Si: C 63.22, H 5.64, N 4.61, S 21.10; Found: C 63.78, H 5.65, N 4.78, S 21.22. MALDI-TOF MS: Calcd. for 1214.29; Found 1214.28.

Synthesis of DTGe(FBTTh$_2$Cy)$_2$: A microwave-assisted Stille coupling between 4,4-bis(2-ethylhexyl)-2,6-bis(trimethylstannyl)-4H-germolo[3,2-b:4,5-b']dithiophene (400 mg, 0.50 mmol) and (532mg, 1.11 mmol) was carried out by using the previous our synthetic condition.[45] The product was purified by

flash chromatography using a hexanes/chloroform as a deep blue solid. Yield: 235 mg (37%). ^{1}H NMR (400 MHz, CDCl$_3$) δ 8.33 (s, 2H), 7.98 (s, 2H), 7.66 (d, J = 8.0 Hz, 2H), 7.14 (dd, J = 4.0, 8.0 Hz, 2H), 7.10 (d, J = 4.0Hz, 2H), 6.73 (s, 2H), 2.80 (br s, 2H), 2.08 – 1.63(m, 12H), 1.49 – 1.20 (m, 30H), 0.87 (m, 12H). ^{13}C NMR (100 MHz, CDCl$_3$) δ 152.75, 149.69, 147.56, 145.61, 140.91, 140.40, 136.05, 133.81, 133.28, 129.79, 128.97, 128.96, 124.56, 123.87, 122.89, 116.23, 115.90, 114.61, 40.00, 39.66, 37.13, 35.67, 35.30, 30.95, 29.11, 28.81, 26.42, 25.93, 23.10, 20.93, 14.20, 10.93. Elemental Analysis Calc. for C$_{64}$H$_{68}$F$_2$GeN$_4$S$_8$: C 60.99, H 5.44, N 4.45, S 20.35; Found: C 61.15, H 5.62, N 4.52, S 20.36. MALDI-TOF MS: Calcd. for 1260.24; Found 1260.23.

Chapter Ⅱ. In-depth study of Introducing the Fluorine Atoms Inhabiting in Accepting Unit.

2.1. Introduction.

Over the past two decades, many studies about bulk heterojunction organic solar cells (OSCs) based on small molecules (SMBHJ) have attracted attention as next generation energy conversion devices due to the many kinds of advantages such like ease of functionalization, mono-diversity and distinct molecular structures and many endeavors have achieved successful increase of power conversion efficiencies (PCE) over the 10% in this field. Among of efforts related with improvements of PCE, alternating donor-acceptor (D-A) molecular architecture that facilitates better charge dissociation on interface between donor and acceptor were well recognized as the most successful approach to access higher PCE.[64]

Among of various donating and accepting units, 5-fluorobenzo[c][1,2,5]thiadiazole (FBT) unit has been widely exploited for the highest performance with many substantiations to be one of the most promising acceptor units resulted from strong electron affinity inducing intramolecular charge transfer (ICT) interactions between donor and acceptor.[8c, 8d] Furthermore, because introducing fluorine (F) atoms which have strong electron-withdrawing ability could suggest methodologies to adjust not only the electronic properties but also noncovalent interactions, many kinds of donor materials incorporated with FBT unit have been emerged in this field.[65] However, although intensive researches have been progressed, only few successful studies about in-depth study of F atoms have been investigated recently.

In this study, we implanted FBT as an acceptor unit into 4,4-bis(2-ethylhexyl)-4H-silolo[3,2-b:4,5-b']dithiophene (DTSi) and 4,4-bis(2-ethylhexyl)-4H-germolo[3,2-b:4,5-b']dithiophene (DTGe) core units with different end capping group as bithiophene (Th$_2$) and benzofuran (BFu). Especially, we attempted to investigate the absorption properties, electro-chemical properties and photovoltaic characteristics with existence of F atoms on different position in FBT unit compared to the well-known 7,7'-(4,4-bis(2-ethylhexyl)-4H-silolo[3,2-b:4,5-b']dithiophene-2,6-diyl)bis(6-fluoro-4-(5'-hexyl-[2,2'-bithiophen]-5-yl)benzo[c][1,2,5]thiadiazole) (DTSi(FBTTh$_2$)$_2$), 7,7'-(4,4-bis(2-ethylhexyl)-4H-germolo[3,2-b:4,5-b']dithiophene-2,6-diyl)bis(6-fluoro-4-(5'-hexyl-[2,2'-bithiophen]-5-yl)benzo[c][1,2,5]thiadiazole) (DTGe(FBTTh$_2$)$_2$), 7,7'-(4,4-bis(2-ethylhexyl)-4H-silolo[3,2-b:4,5-b']dithiophene-2,6-diyl)bis(4-(benzofuran-2-yl)-6-fluorobenzo[c][1,2,5]thiadiazole) (DTSi(FBTBFu)$_2$) and 7,7'-(4,4-bis(2-ethylhexyl)-4H-germolo[3,2-b:4,5-b']dithiophene-2,6-diyl)bis(4-(benzofuran-2-yl)-6-fluorobenzo[c][1,2,5]thiadiazole) (DTGe(FBTBFu)$_2$).

2.2. Results and Discussion.

2.2.1. Synthesis and characterization.
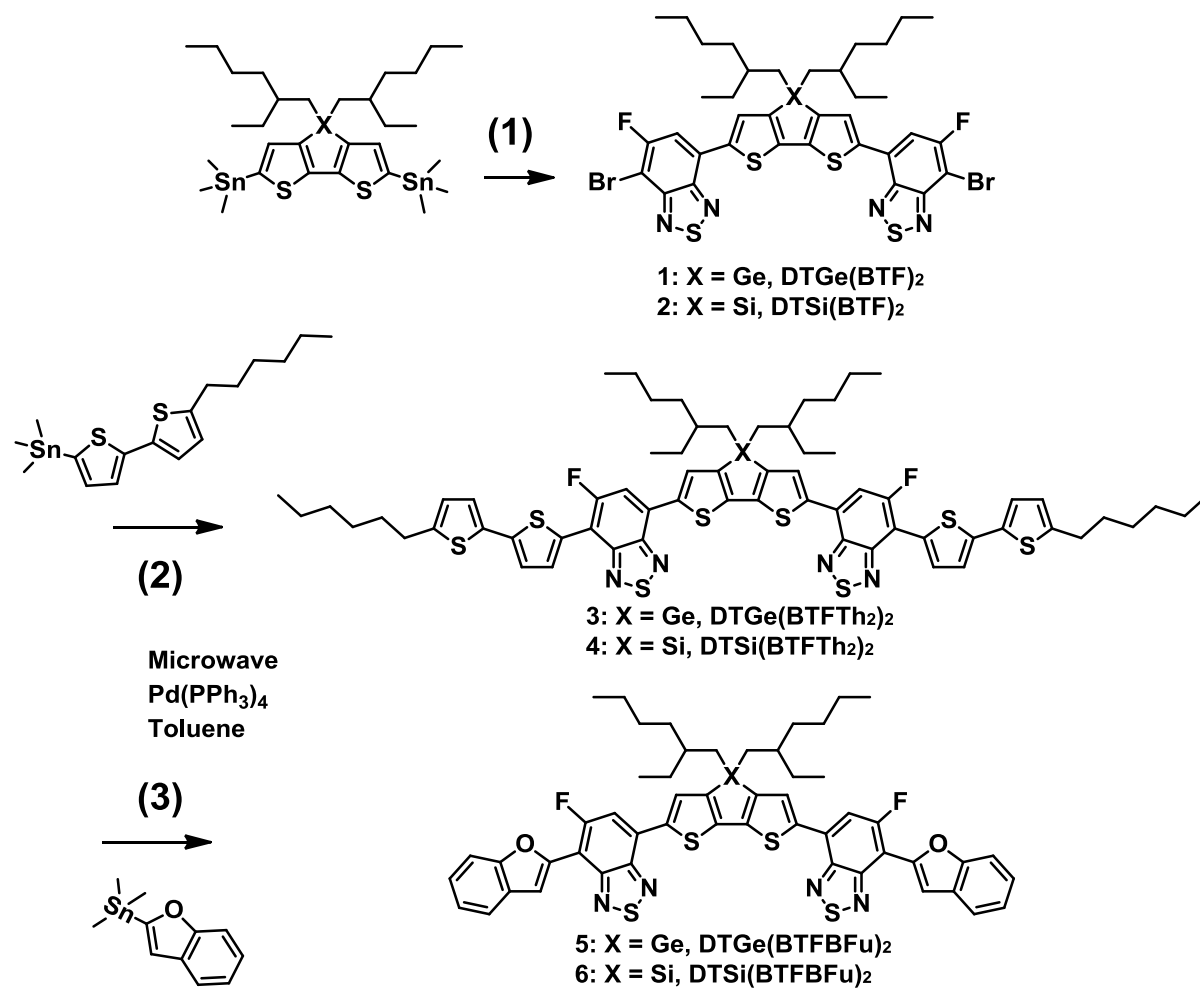
Figure 19. Illustrated synthetic pathways for the final target molecules.

The key reactions for the final compounds are shown in **Figure 19**. The key steps of (1), (2) and (3) were accomplished through the common microwave assisted Stille coupling and each intermediates and detailed experimental procedures were described in experimental section. Finally, final four small molecules of 7,7'-(4,4-bis(2-ethylhexyl)-4H-silolo[3,2-b:4,5-b']dithiophene-2,6-diyl)bis(5-fluoro-4-(5'-hexyl-[2,2'-bithiophen]-5-yl)benzo[c][1,2,5]thiadi-azole) (DTSi(BTFTh$_2$)$_2$), 7,7'-(4,4-bis(2-ethylhexyl)-4H-germolo[3,2-b:4,5-b']dithiophene-2,6-diyl)bis(5-fluoro-4-(5'-hexyl-[2,2'-bithiophen]-5-yl)benzo[c][1,2,5]thiadiazole) (DTGe(BTFTh$_2$)$_2$), 7,7'-(4,4-bis(2-ethylhexyl)-4H-silolo[3,2-b:4,5-b']dithiophene-2,6-diyl)bi-s(4-(benzofuran-2-yl)-5-fluorobenzo[c][1,2,5]thiadiazole) (DTSi(BTFBFu$_2$)) and 7,7'-(4,4-bis(2-ethylhexyl)-4H-germolo[3,2-b:4,5-b']dithiophene-2,6-diyl)bis(4-(benzofuran-2-yl)-5-fluorobenzo[c][1,2,5]thiadiazole) (DTGe(BTFBFu$_2$)) could be acquired

28

with different two end capping groups respectively. The structures and purity were completely confirmed by ^{1}H, ^{13}C nuclear magnetic resonance (NMR) spectroscopy, matrix assisted laser desorption/ionization time-of-flight (MALDI-TOF) spectroscopy and elemental analysis (EA). All target compounds of DTSi(BTFTh$_2$)$_2$, DTGe(BTFTh$_2$)$_2$, DTSi(BTFBFu)$_2$ and DTGe(BTFBFu)$_2$ exhibited good solubility in general organic solvents.

2.2.2. Molecular Conformation and Dipole Momentum.

To understand induced effects by existence of F atoms on different position in FBT unit, we firstly calculated molecular conformation and dipole moment of ground state through the density functional theory (DFT) with DTSi(FBTTh$_2$)$_2$, DTGe(FBTTh$_2$)$_2$, DTSi(FBTBFu)$_2$ and DTGe(FBTBFu)$_2$ (**Figure 20**.) in this section. Interestingly, all compounds of DTSi(BTFTh$_2$)$_2$, DTGe(BTFTh$_2$)$_2$, DTSi(BTFBFu)$_2$ and DTGe(BTFBFu)$_2$ which F atoms head for end capping groups exhibited coplanar molecular conformations along the backbone and higher net dipole moments in ground state compared to the what F atoms head for opposite directions.

a)
DTSi(BTFTh$_2$)$_2$ **DTSi(FBTTh$_2$)$_2$**
Side view   Side view
Dipole = 1.4615 Debye   Dipole = 0.2905 Debye

b)
DTGe(BTFTh$_2$)$_2$ **DTGe(FBTTh$_2$)$_2$**
Side view   Side view
Dipole = 1.6535 Debye   Dipole = 0.4250 Debye

30
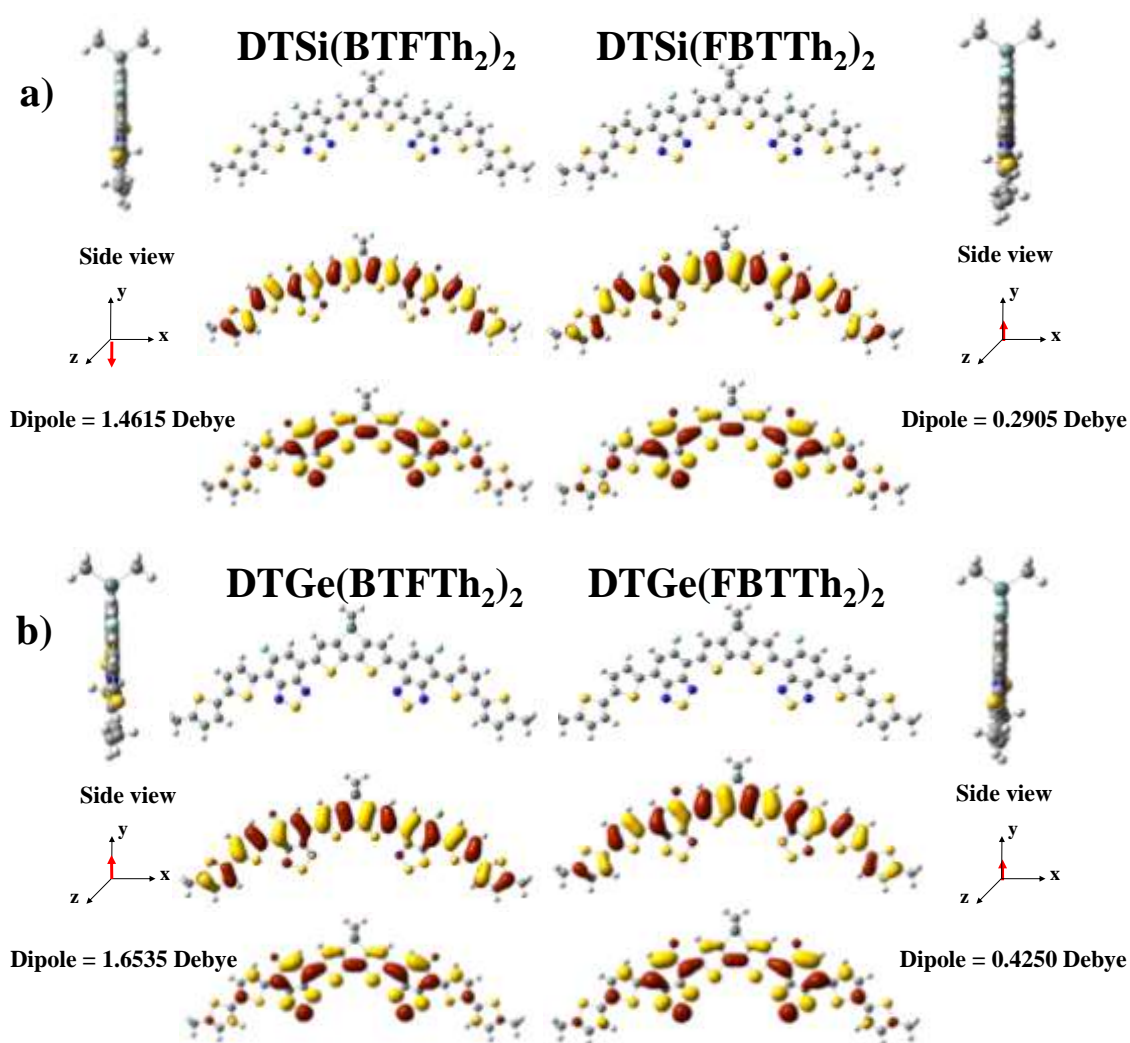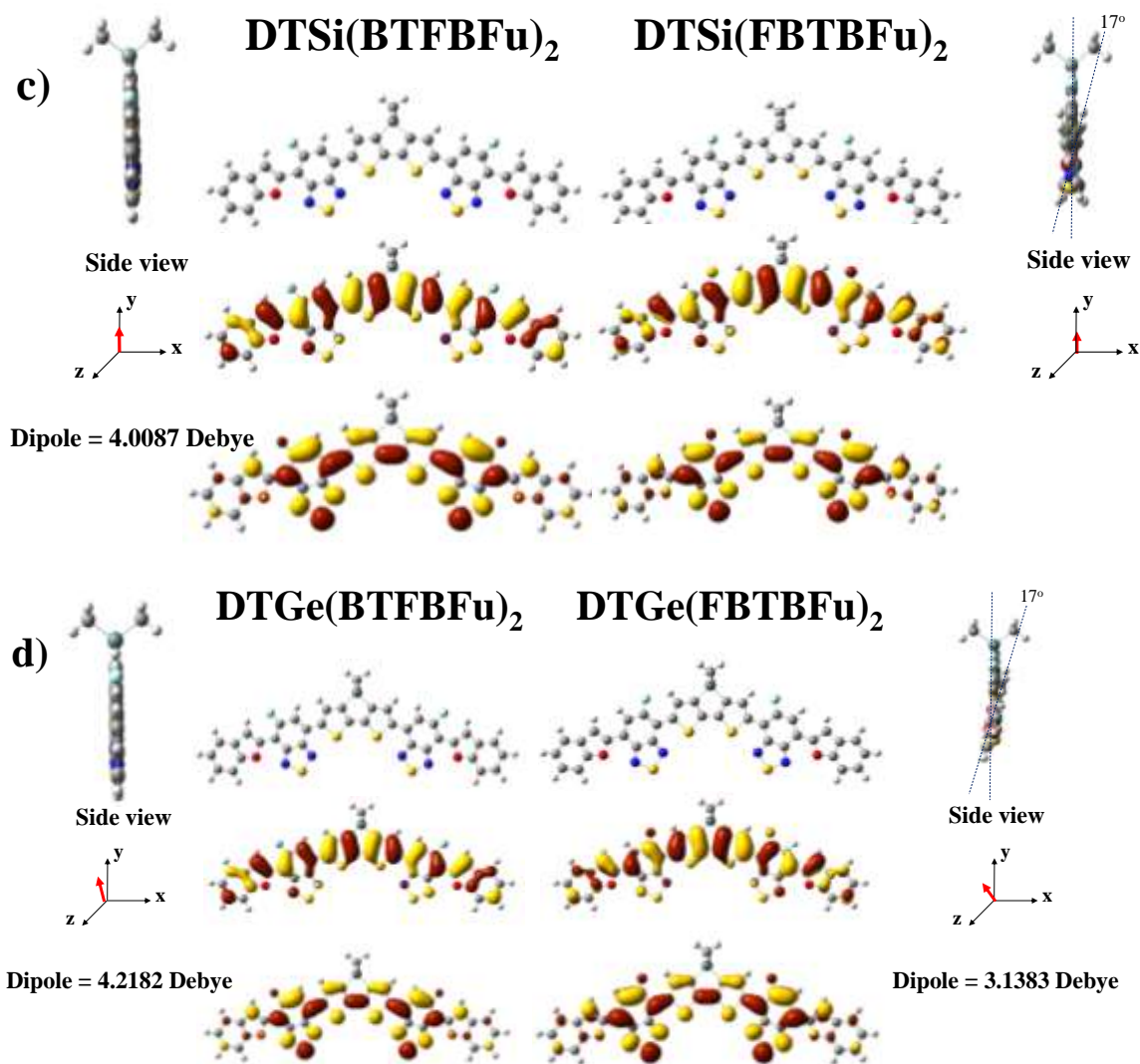
Figure 20. Molecular conformations and dipole moments calculated by DFT.

These results inferred that non-covalent interactions of F atoms between core units and different end capping group affect not only their planarity but also polarization of delocalized electron of ground state and it would lead different driving forces for the charge tranporting when it is exposed to environment to induce photovoltaic effect depends on location of F atom.[66] Especially, DTSi and DTGe moieties end-capped with BFu exhibited distinct differences of planarity by ≈ 15°. It seems that F atoms of DTSi(BTFBFu)$_2$ and DTGe(BTFBFu)$_2$ could amicable overlap oxygen atom in benzofuran.

2.2.3. Optical and Electro-Chemical Properties.

We measured UV-Vis spectroscopy all compounds of DTSi(BTFTh$_2$)$_2$, DTGe(BTFTh$_2$), DTSi(BTFBFu)$_2$ and DTGe(BTFBFu)$_2$ as solution state and film state and their absorption spectra are shown in **Figure 21**.
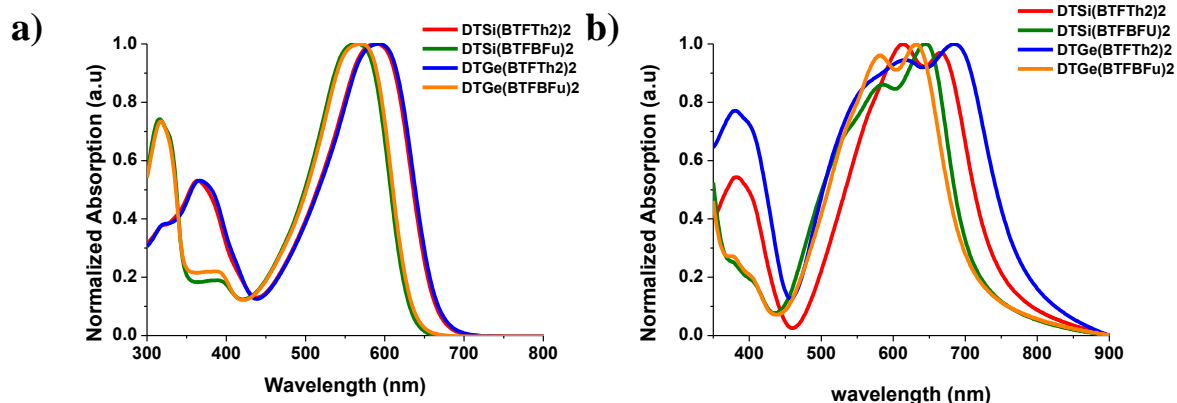
Figure 21. UV-vis spectrum of DTSi(BTFTh$_2$)$_2$, DTGe(BTFTh$_2$)$_2$, DTSi(BTFBFu)$_2$ and DTGe(BTF-BFu)$_2$ as solution state a) dissolving in chloroform and film state b).

In solution state, both compounds of DTSi(BTFTh$_2$)$_2$ and DTGe(BTFTh$_2$)$_2$ exhibited slightly red-shifted λ_{max} at 563, 565 nm respectively compared to the DTSi(BTFBFu)$_2$ and DTGe(BTFBFu)$_2$ in chloroform. On the other hand, λ_{max} of all compounds exhibited bathochromic shift by $\approx$ 121 nm on film state indicating ordered packing. Especially, λ_{max} of DTSi(BTFBFu)$_2$ (λ_{max}: 642nm) and DTGe(BTFTh$_2$)$_2$ (λ_{max}: 686nm) are greater than the red-shift of DTSi(BTFTh$_2$)$_2$ (λ_{max}: 611nm) and DTGe(BTFBFu)$_2$ (λ_{max}: 630nm) noting that facilitate greater electronic delocalization in the solid state. And we calculated time dependent (TD) DFT for the understanding the nature of charge transfer optical transition on the gas phase and the results are shown in **Figure 22**. These TD-DFT results indicated that main excited transition at 771 and 688 nm for the DTSi(BTFTh$_2$)$_2$ and DTGe(BTFTh$_2$)$_2$ with an oscillator strength 0.637 and 0.636 respectively and 687, 772nm for the DTSi(BTFBFu)$_2$, DTGe(BTFBFu)$_2$ with 0.636, 0.637 oscillator strength on the solid state.
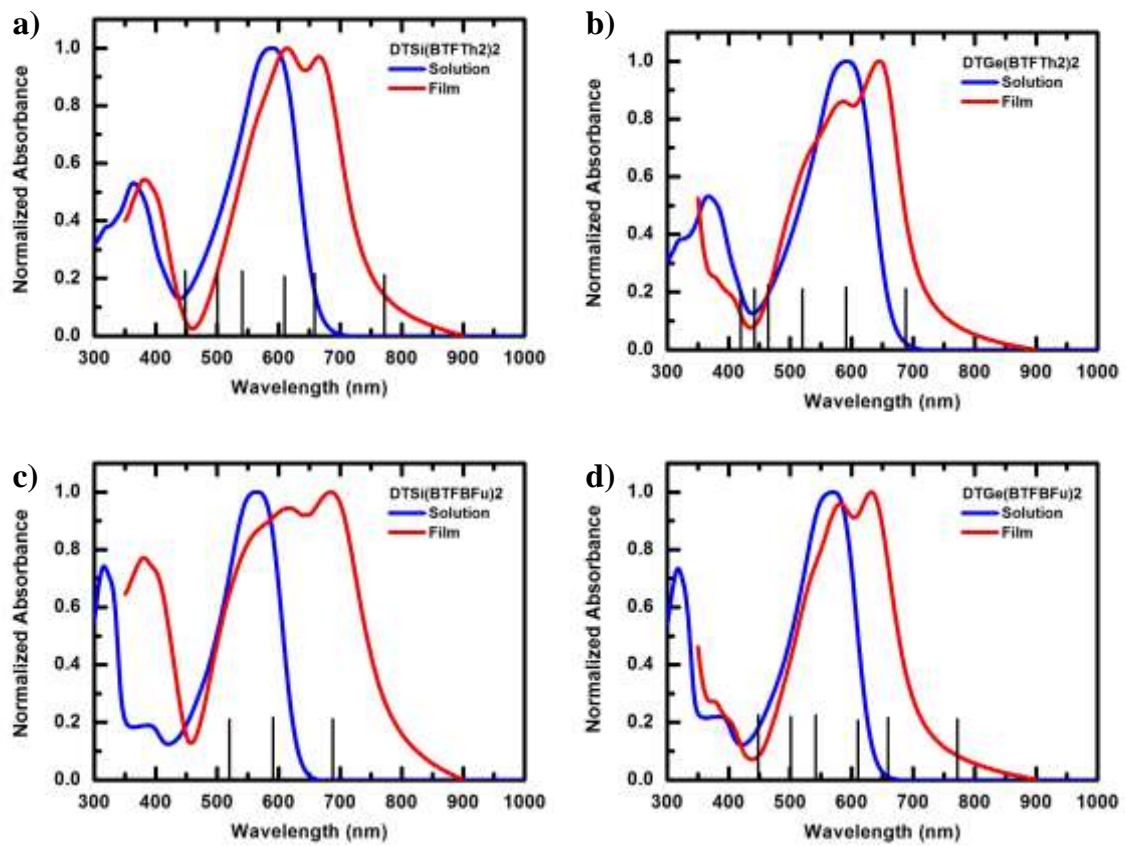
Figure 22. Transition absorption spectra of a) DTSi(BTFTh$_2$)$_2$, b) DTGe(BTFTh$_2$)$_2$, c) DTSi(BTFBFu)$_2$ and d) DTGe(BTFBFu)$_2$ calculated by time dependent DFT.

And we measured cyclic voltammetry (CV) of solution state to understand electro-chemical properties as an external process and cyclic voltammograms are described in **Figure 23**.
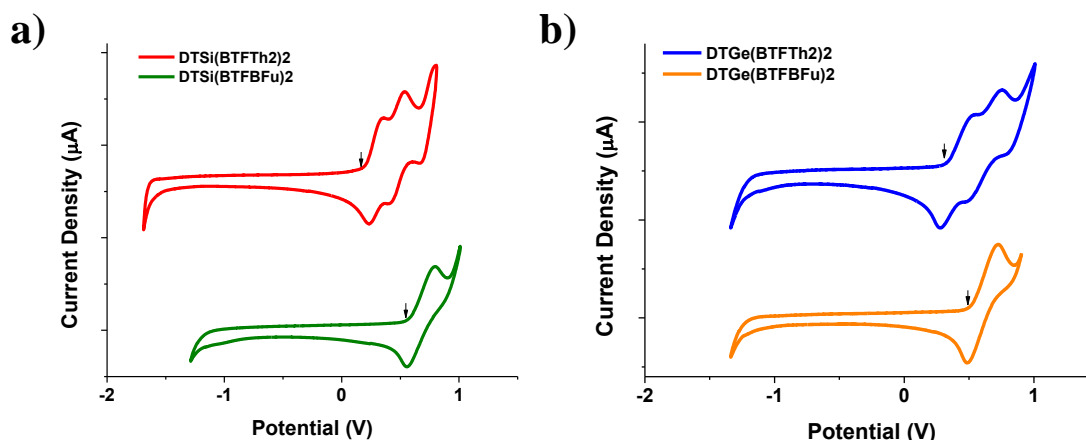
Figure 23. Cyclic voltammograms of DTSi(BTFTh$_2$)$_2$, DTSi(BTFBFu)$_2$, DTGe(BTFTh$_2$)$_2$ and DTGe(BTFBFu)$_2$ in n-Bu4NPF$_6$/CHCl$_3$ solutions with external reference measurement of ferrocene (scan rate: 100 mV s^{-1}).

While all compounds exhibited distinct oxidation peaks reversely, peak of reduction indicating lowest occupied molecular orbital (LUMO). For this reason, each LUMO values were calculated with optical band gap and calculated frontier orbital energies by cyclic voltammetry and DFT were shown in **Table 4**.

Table 4. Summaries of energy levels calculated by CV results and DFT.

Material	HOMO [eV]	LUMO [eV]	E_g [eV]
DTSi(BTFTh$_2$)$_2$ (CV)	-4.94	-3.14	1.80
DTSi(BTFTh$_2$)$_2$ (DFT)	-4.70	-2.87	1.83
DTGe(BTFTh$_2$)$_2$ (CV)	-5.08	-3.27	1.81
DTGe(BTFTh$_2$)$_2$ (DFT)	-4.70	-2.87	1.83
DTSi(BTFBFu)$_2$ (CV)	-5.32	-3.39	1.93
DTSi(BTFBFu)$_2$ (DFT)	-4.91	-2.91	2.00
DTGe(BTFBFu)$_2$ (CV)	-5.25	-3.33	1.92
DTGe(BTFBFu)$_2$ (DFT)	-4.86	-2.90	1.96

Highest occupied molecular orbital (HOMO) from solution cyclic voltammetry for the compounds of DTSi(BTFBFu)$_2$ and DTGe(BTFBFu)$_2$ exhibited -5.32 and -5.25 eV respectively. These deeper HOMO values coincided well with previously reported effect of incorporating benzofuran moieties compared to the DTSi(BTFTh$_2$)$_2$ and DTGe(BTFTh$_2$)$_2$. On the other hand, although DTSi(BTFTh$_2$)$_2$ and DTGe(BTFTh$_2$)$_2$ recorded reduced energy band gap at 1.80 and 1.83 eV inferring the charge generation ability with less photon energy, changing the central bridgehead atom does not affect their electrochemical properties.

2.2.4. Device Fabrication and Thin Film Morphology.

Conventional solar cell devices were prepared with [6,6]-phenyl-C71-butyric acid methyl ester ($PC_{71}BM$) as an acceptor and fabrication details of device were described in experimental section. After device optimizations related with ratio between donor and acceptor, coating speed rate and blending solution concentration, device tests were progressed under 100 mW cm^{-2} AM 1.5G solar illumination. The results of optimized devices, *J-V* curves and incident photon-to-current efficiency (IPCE) were shown **Figure 24** and **Table 5**.

Table 5. Device characteristics of optimized blend films with $PC_{71}BM$.

Material	Small molecule:$PC_{71}BM$			
	J_{sc} [mA/cm^2]	V_{OC} [V]	FF	PCE [%]
DTSi(BTFTh$_2$)$_2$	10.03	0.79	0.41	3.26
DTGe(BTFTh$_2$)$_2$	6.90	0.81	0.38	2.13
DTSi(BTFBFu)$_2$	8.75	0.85	0.36	2.66
DTGe(BTFBFu)$_2$	5.79	0.83	0.30	1.45
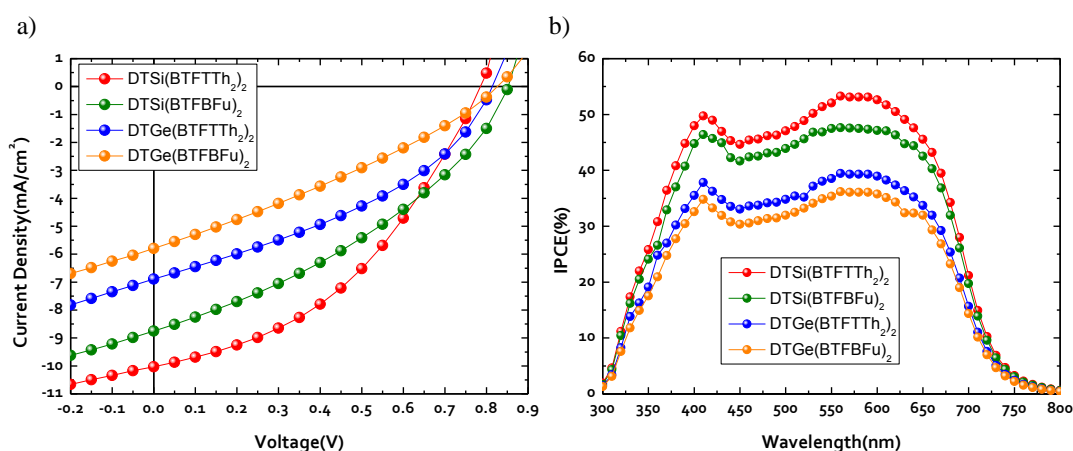
Figure 24. *J-V* curves and IPCE records under optimized device conditions.

Especially, optimized blend film of DTSi(BTFTh$_2$)$_2$ exhibited with short-circuit current density (J_{sc}), open circuit voltage (V_{OC}) and fill factor FF of 10.03 mA/cm^2, 0.79V and 41% yielding a PCE of 3.26%. Although V_{OC} values of all compounds were estimated to be comparable, FF and J_{sc} attributed to morphology, miscibility exhibited significant changes. And each compound of DTSi(BTFTh$_2$)$_2$, DTGe(BTFTh$_2$)$_2$, DTSi(BTFBFu)$_2$ and DTGe(BTFBFu)$_2$ exhibited similar tendency of IPCE depends

36

on wavelength from 350 to 700nm. Furthermore, both compounds of DTSi(BTFTh$_2$)$_2$ and DTSi(BTFTh$_2$)$_2$ which incorporated with Si atom in central bridge head could accomplish the better photon harvesting ability compared to the Ge containing DTGe(BTFTh$_2$)$_2$ and DTGe(BTFBFu)$_2$ and these results agree with higher J_{sc} values of DTSi(BTFTh$_2$) and DTGe(BTFTh$_2$)$_2$ indicating that currents occurred from incident photon could reach to the electrodes without significant loss.

To understand nature of morphology about pristine components, grazing incidence wide angle x-ray diffraction (GIWAXD) were recorded and images and line cuts along the in-plane and out-of-plane directions were described in **Figure 25** and **Figure 26**.
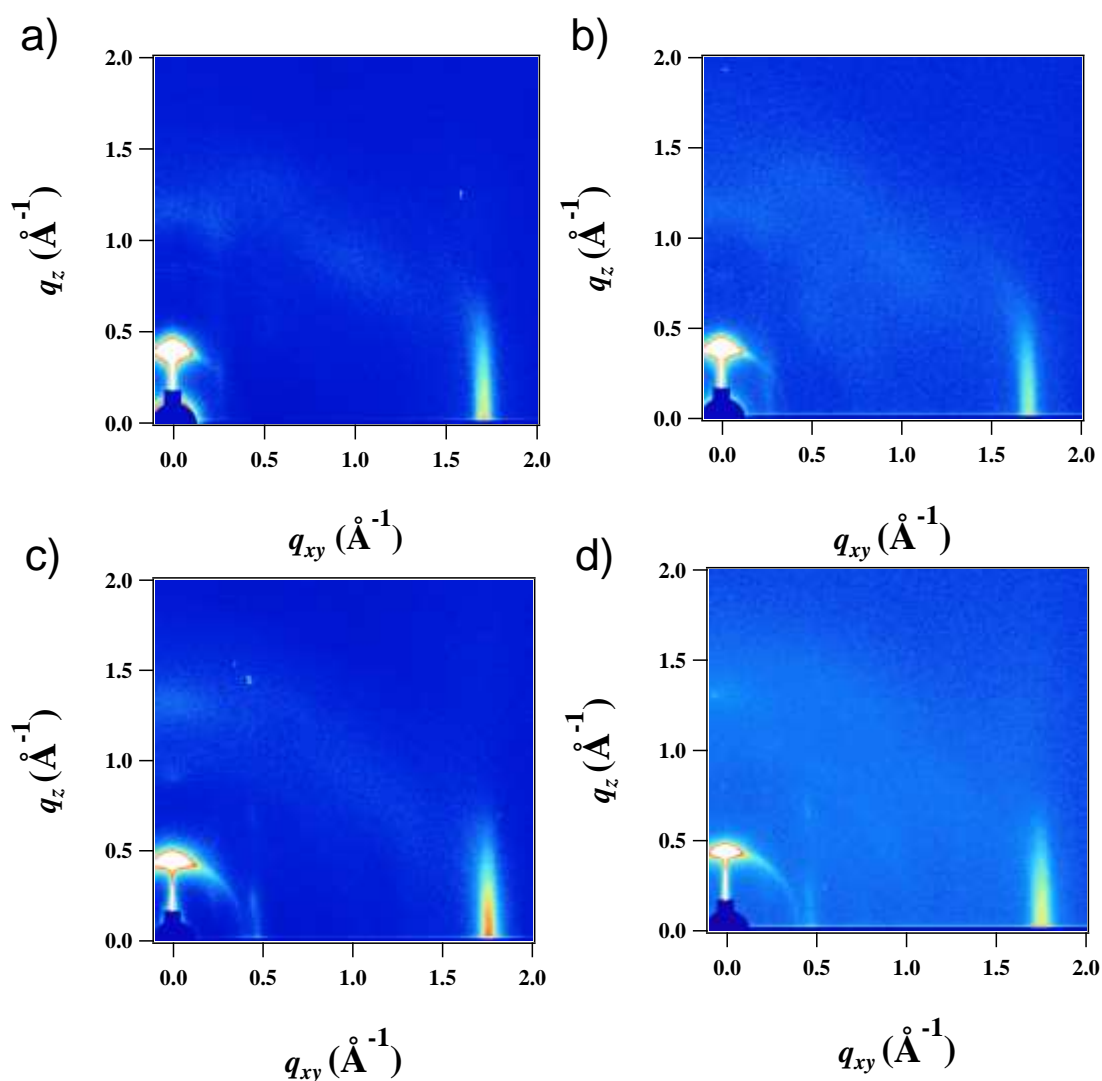
Figure 25. GIWAXS images of a) DTSi(BTFTh$_2$)$_2$, b) DTSi(BTFBFu)$_2$, c) DTGe(BTFTh$_2$)$_2$ and d) DTGe(BTFBFu)$_2$ as a pristine component.

The GIWAXD patterns of all compounds exhibited not formulaic packing orientation unformulaic molecular packing orientations except for the slight lamellar and π-π stacking orientation.
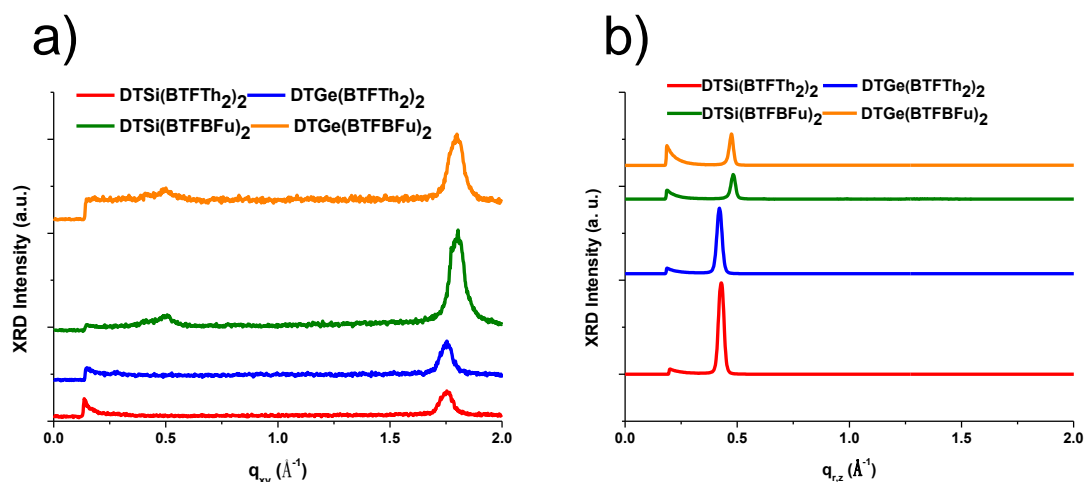
Figure 26. Line cuts corresponds to GIWAXS patterns along the in-plane a) and out-of-plane b).

Interestingly, both distances of lamellar and π-π stacking for the DTSi(BTFTh$_2$)$_2$ and DTGe(BTFTh$_2$)$_2$ exhibited longer distances at 14.68, 14.81, 3.58 Å respectively. On the other hand, BFu containing small molecules exhibited packing distances 13.03, 13.17 and 3.48 Å depends on axis. These results indicated that although end capping group of Th$_2$ induce the steric hindrance due to their rigidity, compounds were capable of efficient packing with each other leading to higher PCE. Furthermore, differences of packing orientation were not exhibited depends on central atoms.

Table 6. Summaries of crystallo-properties acquired from GIWAXS patterns.

Film	Lamellar			π-π stacking		
	q_z (Å^{-1})	d-spacing (Å)		q_{xy} (Å^{-1})		d-spacing (Å)
DTSi(BTFTh$_2$)$_2$	0.428	14.6803395		1.754		3.58220371
DTGe(BTFTh$_2$)$_2$	0.424	14.81883327		1.754		3.58220371
DTSi(BTFBFu)$_2$	0.482	13.03565416		1.801		3.488720326
DTGe(BTFBFu)$_2$	0.477	13.17229624		1.802		3.486784299

We also measured atomic force microscopy (AFM) to understand bulk and surface morphology and images of AFM described in **Figure 27**.
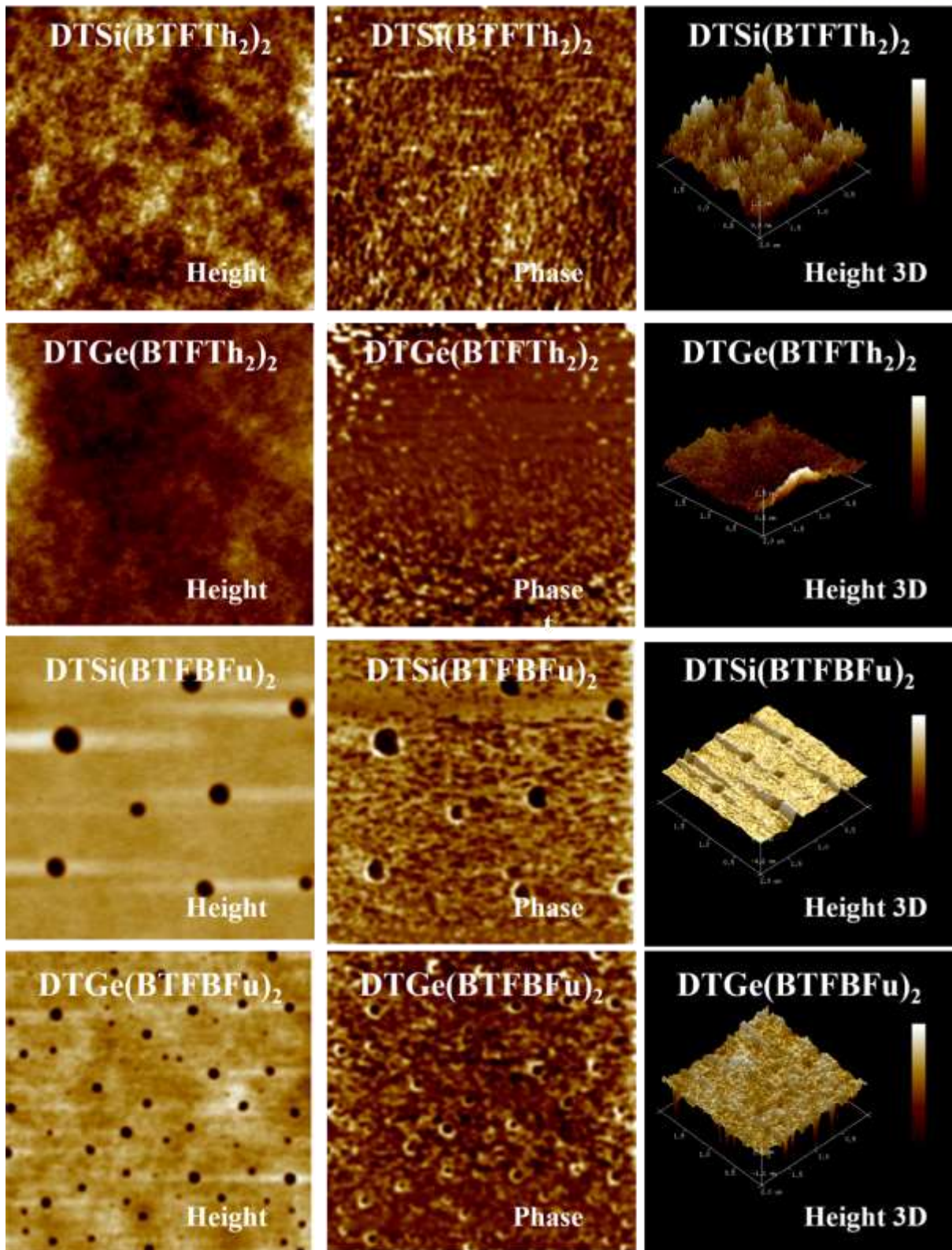
Figure 27. AFM images of DTSi(BTFTh$_2$)$_2$, DTSi(BTFBFu)$_2$, DTGe(BTFTh$_2$)$_2$ and DTGe(BTFBFu)$_2$

Especially, AFM image of DTSi(BTFTh$_2$)$_2$ showed fibril-like structures leading the improved J_{sc} and

FF. However, BFu containing small molecules exhibited pin hole phenomenon in AFM images. These results indicated that when devices were fabricated, solvents could not be evaporated without hitch due to the aggregation with each other caused by miscibility.[67] As a result, it leaded dramatic decay of device performance.

2.3. Conclusion.

We attempted to understand effect of introducing F atoms onto the BT accepting unit and their optical, electrochemical properties and photovoltaic effect. For these reason, we have synthesized four small molecules (DTSi(BTFTh$_2$)$_2$, DTGe(BTFTh$_2$)$_2$, DTSi(BTFBFu)$_2$ and DTGe(BTFBFu)$_2$ successfully. Among of them, DTSi(BTFTh$_2$)$_2$ recorded highest PCE at 3.26 % with higher J_{sc} (10.03 mA/cm^2) and FF (0.41). Furthermore, although Th$_2$ containing small molecules which have longer distances of crystal along the both axis, they could form the effective packing orientation for the charge transporting leading the improvements of device characteristics. However, despite more planar molecular structures of BFu containing family with shorter distances of crystal, they exhibited lower device performance. These results based on aggregation caused by inter molecular interaction could be confirmed through the pin hole phenomenon in AFM images. However, further investigations are needed for the understating effects of incorporating F atoms and rational design for conjugated molecules.

41

2.4. Experimental Section

Materials and Instruments: All the chemicals and reagents were purchased from either Sigma Aldrich, Alfa Aesar Chemical Company, and Solarmer and used without further purification. All solvents are ACS and anhydrous grade by distillation. ^{1}H NMR and ^{13}C NMR spectra were recorded on an Agilent 400 MHz spectrometer using deuterated $CDCl_3$ as solvent and tetramethylsilane (TMS) as an internal standard. Elementary analyses were carried out with a Flash 2000 element analyzer (Thermo Scientific, Netherlands) and MALDI-TOF MS spectra were checked by Ultraflex III (Bruker, Germany). UV-Vis-NIR absorption spectra in solution and in thin films were measured on a UV-1800 (SHIMADZU) spectrophotometer. Cyclic voltammetry (CV) measurements were performed on AMETEK Versa STAT 3 with a three-electrode cell system in a nitrogen bubbled 0.1 M tetra-*n*-butylammonium hexafluorophosphate (*n*-Bu$_4$NPF$_6$) solution in chloroform at a scan rate of 100 mV/s at room temperature. Ag/Ag$^+$ electrode, platinum wire, and carbon glassy were used as the reference electrode, counter electrode, and working electrode, respectively. The Ag/Ag$^+$ reference electrode was calibrated using a ferrocene/ferrocenium redox couple as an internal standard, whose oxidation potential is set at -4.8 eV with respect to a zero-vacuum level. The HOMO energy levels were obtained from the equation HOMO (eV) = $-$ (E$_{(ox)}$^{onset} $-$ E$_{(ferrocene)}$^{onset} + 4.8). The LUMO levels were obtained from the equation LUMO (eV) = $-$ (E^{opt} $-$ E$_{(ferrocene)}$^{onset} + 4.8). DFT calculations were performed using the Gaussian 09 package with the nonlocal hybrid Becke three-parameter Lee-Yang-Parr (B3LYP) function and the 6-31G basis set to elucidate the HOMO and LUMO levels after optimizing the geometry of small molecules using the same method.

Synthesis of 7,7'-(4,4-bis(2-ethylhexyl)-4H-germolo[3,2-b:4,5-b']dithiophene-2,6-diyl)bis(4-bromo-5-fluorobenzo[c][1,2,5]thiadiazole) **DTGe(BTF)$_2$, (1)** : 30mL microwave tube was charged with 4,4-bis(2-ethylhexyl)-2,6-bis(trimethylstannyl)-4H-germolo[3,2-b:4,5-b']dithio-phene (Me$_3$Sn-DTGe-SnMe$_3$, 1.20 g, 1.52 mmol), 4,7-dibromo-5-fluorobenzo[c][1,2,5]-thiadiazole (FBTBr$_2$, 1.19 g, 3.80 mmol), Pd(PPh$_3$)$_4$ (0.087 g, 0.076 mmol), and toluene (10 mL), under Ar condition. The reaction mixture was heated to 100 ℃ for 1 min, 125 ℃ for 1 min, 150 ℃ for 10 min, and 160 ℃ for 60 min using a Biotage microwave reactor. After cooling, the material was loaded onto silica and purified by flash chromatography using hexanes/chloroform gradient. Solvent was removed after collection. The solid in 3:1 mixture of methanol and hexanes was sonicated for 1 h and stirred during the overnight. The suspension was filtered and recrystallized with dichloromethane and hexane. Finally, red solid was obtained (0.61 g, yield: 43%). ^{1}H NMR (400MHz, CDCl$_3$): δ 8.19 (t, *J* = 8.0 Hz, 2H), 7.68 (d, *J* = 4.0 Hz, 2H), 1.58 (m, 4H), 1.45 − 1.12 (m, 18H), 0.82 (m, 12H). ^{13}C NMR (100MHz, CDCl$_3$): δ 148.92, 148.86, 147.14, 139.03, 132.14, 132.11, 127.71, 127.61, 115.27, 114.96, 37.06,

35.57, 28.98, 28.78, 23.02, 20.92, 14.14, 10.89. Elemental analysis calc. For $C_{36}H_{38}Br_2F_2GeN_4S_4$: C 46.72 H 4.14 N 6.05 S 13.86; Found: C 48.21 H 4.36 N 6.43 S 13.84. MALDI-TOF: Calcld. For 925.42; Found: 925.95.

Synthesis of 7,7'-(4,4-bis(2-ethylhexyl)-4H-silolo[3,2-b:4,5-b']dithiophene-2,6-diyl)bis(4-bromo-5-fluorobenzo[c][1,2,5]thiadiazole) **DTSi(BTF)₂, (2)**: this reaction was progressed in the same method as **DTGe(BTF)₂**. 4,4-bis(2-ethylhexyl)-2,6-bis(trimethylstannyl)-4H-silolo[3,2-b:4,5-b']dithiophene (Me₃Sn-DTSi-SnMe₃, 1.40 g, 1.88 mmol), 4,7-dibromo-5-fluorobenzo[c][1,2,5]-thiadiazole (FBTBr₂, 1.47 g, 4.70 mmol), Pd(PPh₃)₄ (0.108 g, 0.094mmol) and toluene (10 mL) added into 30 mL microwave tube. it was also heated to 100 ℃ for 1 min, 125 ℃ for 1 min, 150 ℃ for 10 min, and 160 ℃ for 60 min using a Biotage microwave reactor. And then, it was followed same purification method. As a result, product was obtained as a dark-red solid (0.42 g, yield: 26%). ¹H NMR (400MHz, CDCl₃): δ 8.17 (t, J = 8.0 Hz, 2H), 7.68 (d, J = 4.0 Hz, 2H), 1.51 (m, 2H), 1.43 – 1.16 (m, 16H), 1.09 (m, 4H), 0.82 (t, 12H). ¹³C NMR (100MHz, CDCl₃): δ 151.25, 148.84, 145.57, 132.10, 132.07, 132.04, 127.69, 127.59, 115.35, 115.04, 35.98, 35.72, 30.91, 28.93, 22.99, 17.64, 14.14, 10.82. Elemental analysis calc. For $C_{36}H_{38}Br_2F_2N_4S_4Si$: C 49.09 H 4.35 N 6.36 S 14.56; Found: C 49.34 H 4.50 N 6.55 S 14.82. MALDI-TOF: Calcld. For 880.86; Found: 880.00.

Synthesis of **DTGe(BTFTh₂)₂, (3)**: Stille coupling between **(1)** (0.4g, 0.432 mmol) and (5'-hexyl-[2,2'-bithiophen]-5-yl)trimethylstannane (Th₂, 0.392g, 0.951 mmol) were progressed in obedience to same procedures of **(1)** with Pd(PPh₃)₄ (0.024 g, 0.022mmol) and 8 mL of toluene. Deep blue solids were acquired at 48% yield. %). ¹H NMR (400MHz, CDCl₃): δ 8.19 (t, J = 3.3 Hz, 2H), 8.11 (d, J = 4.0 Hz, 2H), 7.58 (d, J = 13.1 Hz, 2H), 7.16 (d, J = 4.0 Hz, 2H), 7.09 (d, J = 3.5 Hz, 2H), 6.70 (d, J = 3.5 Hz, 2H), 2.81 (t, J = 7.6 Hz, 4H), 1.68 (m, 6H), 1.50 – 1.20 (m, 32H), 0.94 – 0.81 (m, 18H). ¹³C NMR (100MHz, CDCl₃): δ 153.21, 149.51, 148.71, 146.75, 146.00, 139.78, 134.56, 131.43, 131.41, 131.05, 130.83, 130.73, 125.47, 124.91, 123.72, 123.11, 115.29, 110.54, 37.10, 35.64, 31.58, 31.53, 30.24, 29.05, 28.83, 28.80, 23.10, 22.58, 20.94, 14.21, 14.08, 10.94. Elemental analysis calc. For $C_{64}H_{72}F_2GeN_4S_8$: C 60.79 H 5.74 N 4.43 S 20.29; Found: C 60.79 H 5.80 N 4.54 S 20.15. MALDI-TOF: Calcld. For 1264.27; Found: 1264.27.

Synthesis of **DTSi(BTFTh₂)₂, (4)**: Stille coupling between **(2)** (0.4g, 0.454 mmol) and (5'-hexyl-[2,2'-bithiophen]-5-yl)trimethylstannane (Th₂, 0.413g, 0.999 mmol) were progressed in obedience to same procedures of **(3)** with Pd(PPh₃)₄ (0.024 g, 0.022mmol) and 8 mL of toluene. Deep blue solids were acquired at 35% yield. ¹H NMR (400MHz, CDCl₃): 8.19 (t, J = 4.0 Hz, 2H), 8.15 (d, J = 4.0 Hz, 2H), 7.66 (d, J = 12.0 Hz, 2H, 7.19 (d, J = 4.0 Hz, 2H), 7.11 (d, J = 4 Hz, 2H), 6.72 (d, J = 8.0 Hz, 2H), 2.81 (t, J = 8.0Hz, 4H), 1.71 (m, 4H), 1.56 (m, 2H), 1.47 – 1.04 (m, 32H), 0.96 – 0.77 (m, 18H). ¹³C

NMR (100MHz, CDCl$_3$): δ 156.32, 154.43, 149.37, 148.82, 144.00, 142.78, 138.56, 136.43, 134.28, 132.37, 131.83, 131.69, 128.45, 124.85, 121.63, 120.13, 112.39, 110.65, 36.10, 34.64, 33.58, 32.53, 31.28, 29.37, 28.75, 28.65, 22.80, 22.53, 20.43, 14.11, 13.08, 10.87. Elemental analysis calc. For C$_{64}$H$_{72}$F$_2$N$_4$S$_8$Si: C 63.01 H 5.95 N 4.59 S 21.03; Found: C 63.09 H 6.09 N 4.68 S 20.12. MALDI-TOF: Calcld. For 1218.33; Found: 1218.35.

Synthesis of **DTGe(BTFBFFu)$_2$, (5)**: Stille coupling between **(1)** (0.4g, 0.432 mmol) and benzofuran-2-yltrimethylstannane (BFu, 0.267g, 0.951 mmol) were progressed in obedience to same procedures of **(3)** with Pd(PPh$_3$)$_4$ (0.024 g, 0.022mmol) and 8 mL of toluene. purple solids were acquired at 46% yield. ^{1}H NMR (400MHz, CDCl$_3$): δ 8.26 (t, J = 4.0Hz, 2H), 7.91 (s, 2H), 7.77 (d, J = 12.0 Hz, 1H), 7.70 (d, J = 8.0 Hz, 2H), 7.65 (d, J = 8.0 Hz, 2H), 7.37 (t, J = 8.0 Hz, 2H), 7.29 (t, J = 8.0 Hz, 2H), 1.55 (m, 4H), 1.48 – 1.14 (m, 16H), 0.97 – 0.77 (m, 12H). ^{13}C NMR (100MHz, CDCl$_3$): δ 153.89, 153.75, 150.59, 149.33, 144.25, 143.16, 130.42, 126.75, 126.34, 124.25, 121.37, 120.15, 115.37, 113.22, 112.15, 110.97, 110.45, 110.21, 35.01, 33.85, 32.11, 29.86, 25.13, 19.82, 14.32, 11.79. Elemental analysis calc. For C$_{52}$H$_{48}$F$_2$GeN$_4$O$_2$S$_4$: C 62.46 H 4.84 N 5.60 S 12.83; Found: C 64.18 H 5.58 N 6.04 S 11.08. MALDI-TOF: Calcld. For 1000.18; Found: 1000.19.

Synthesis of **DTSi(BTFBFFu)$_2$, (6)**: Stille coupling between **(2)** (0.4g, 0.454 mmol) and benzofuran-2-yltrimethylstannane (BFu, 0.280g, 0.999 mmol) were progressed in obedience to same procedures of **(3)** with Pd(PPh$_3$)$_4$ (0.024 g, 0.022mmol) and 8 mL of toluene. Purple solids were acquired at 38% yield. ^{1}H NMR (400MHz, CDCl$_3$): δ 8.24 (t, J = 4.4 Hz, 2H), 7.90 (s, 2H), 7.75 (d, J = 12 Hz, 2H), 7.69 (d, J = 8 Hz, 2H), 7.65 (d, J = 8.0 Hz, 2H), 7.37 (t, J = 8.0 Hz, 2H), 7.29 (t, J = 8.0 Hz, 2H), 1.58 – 1.54 (m, 6H), 1.44 – 1.05 (m, 16H), 0.89 – 0.77 (m, 12H). ^{13}C NMR (100MHz, CDCl$_3$): 154.98, 154.96, 151.60, 149.64, 146.49, 143.43, 131.99, 128.50, 125., 123.13, 121.42, 121.39, 116.08, 115.77, 114.42, 111.44, 110.07, 110.01, 36.02, 35.76, 30.91, 28.96, 23.03, 17.72, 14.18, 10.85. Elemental analysis calc. For C$_{52}$H$_{48}$F$_2$N$_4$O$_2$S$_4$Si: C 65.38 H 5.06 N 5.86 S 13.43; Found: C 64.99 H 5.45 N 6.59 S 12.44. MALDI-TOF: Calcld. For 954.24; Found: 954.23.

Chapter Ⅲ. Investigation of Effects Induced by Replacements of C-C covalent bond with B←N coordination bond on heteroaromatic compound.

3.1. Introduction.

Over the past two decades, conjugated molecules have attracted attention as a class of semiconducting materials and have been widely used in various fields, such as organic light emitting diodes (OLEDs), organic field-effect transistors (OFETs) and organic solar cells (OSCs) with exotic properties caused by delocalized π-electrons existing along the backbone. Despite many attempts to understand the conjugated molecules, many crucial issues have been remained related with rational design for the desirable properties. One of them is the creation building blocks which have not only reasonably high electron affinity but also crystalline structures for the smooth carrier transport on solution process. As a result of this matter, many researchers have attempted to acquire novel building blocks suggesting guide line for the rational design in these fields. Especially, embedding the hetero atoms (e.g., fluorine (F), nitrogen (N), boron (B)) onto the π-conjugated framework could be one of the most effective methodology for the intrinsic high electron affinity and have been widely accepted with ease of modulating the electro chemical properties, absorption properties even though solid structures. Furthermore, Klaus Müllen et al. demonstrated recently that sequence of embedded B and N atoms could be methodology to tune their aromaticity and it leads changes of optoelectronic properties. Despite many kinds of endeavors related with introducing the B and N atoms which have isoelectronic bond and isosterism with C=C bond onto the conjugated units, many studies have focused covalently linked B, N atoms with carbon atoms and only few successful examples related with embedding the coordinately linked B←N units. In this contribution, we have attempted to design exotic π-conjugated polymer and investigated their optoelectronic properties.

3.2. Result and Discussion.

Herein, we described synthetic routes and characterization with ^{1}H nuclear magnetic resonance (NMR) spectroscopy. Firstly, designated π-conjugated polymer and synthetic pathways were shown in **Figure 28**.

a)

b)
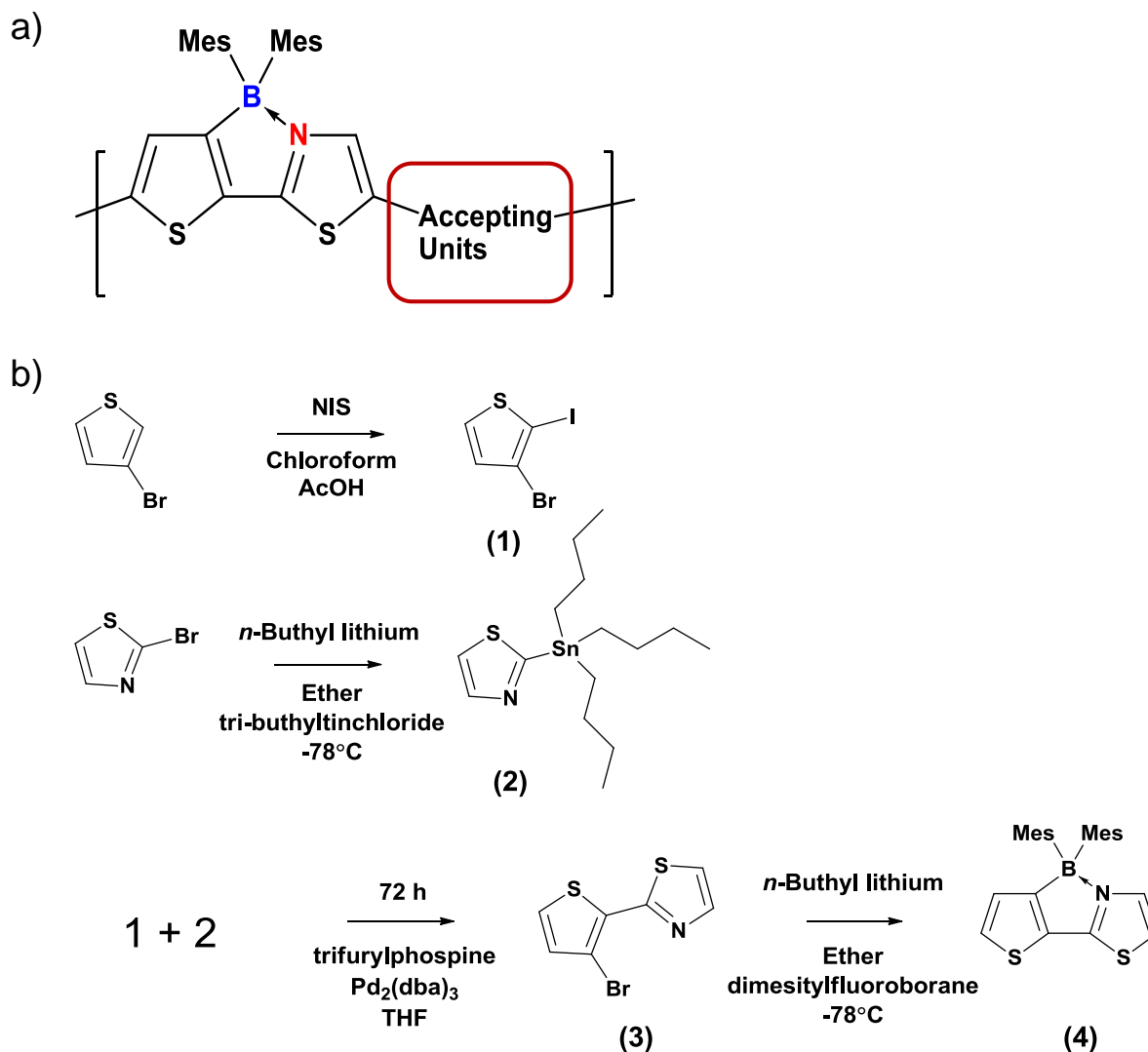
Figure 28. Final target structure a) of molecules incorporated with B←N unit and b) synthetic pathways for the final compounds.

Synthesis of 3-bromo-2-iodothiophene **(1):** *N*-Iodosuccinimide (11.04g, 49.07 mmol was poured into the solution of 3-bromothiophene (10g, 61.33 mmol) solutions dissolving in mixed chloroform with acetic acid at room temperature. The reaction mixtures were stirred for the 1 day with blocking the light. And then, crude mixtures were extracted with ether and purified with prep JAI gel permission chromatography (GPC). After collect product fraction, finally colorless oil was acquired at 68% yield. ^{1}H NMR (400 MHz, CDCl$_3$) δ 7.40 (d, 1H, *J* = 5.5 Hz), 6.90 (d, 1H, *J* = 5.5 Hz).
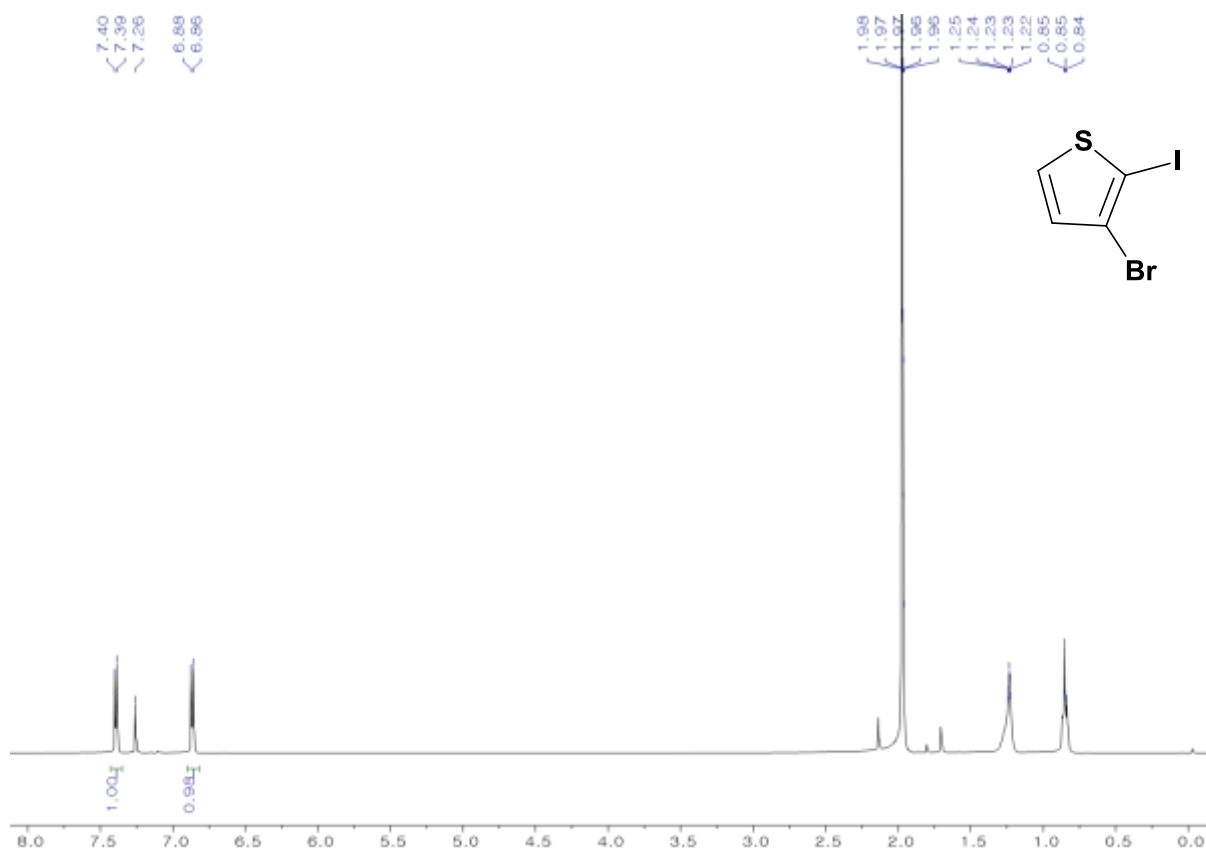
Figure 29. ^{1}H NMR spectra of 3-bromo-2-iodothiophene.

Synthesis of 2-(tributylstannyl)thiazole (**2**): The reaction mixture of 2-bromothiazole (8g, 48.77 mmol) dissolving in ether was cooled down to -78°C thoroughly. And then, *n*-BuLi (1.6M in hexane, 30.48 mL, 48.88 mmol) was added as a dropwise into the reaction mixture. After stirred for the 1.5 h, tri-buthyltinchloride was added and warmed to room temperature. After crude gained from extraction with ether passthrough the short column filled with aluminum oxide, final pale-yellow liquid was acquired through the collection of prep JAI GPC at 65% yield. ^{1}H NMR (400 MHz, CDCl$_3$) δ 8.10 (d, 1H, *J* = 4.0 Hz), 7.54 (d, 1H, *J* = 4.0 Hz).
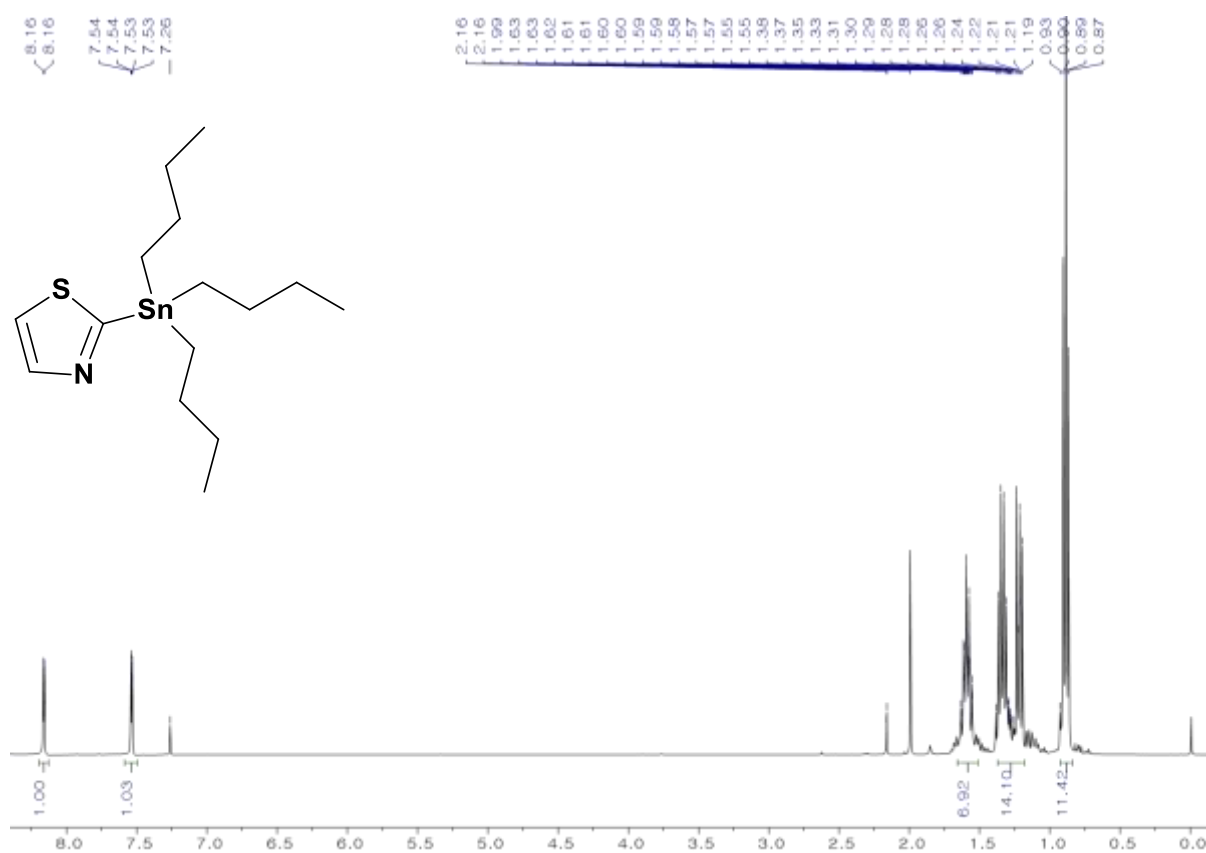
Figure 30. ^{1}H NMR spectra of 2-(tributylstannyl)thiazole.

Synthesis of 2-(3-Bromo-2-thienyl)thiazole **(3)**: Previously prepared **(1)** (5g, 17.31 mmol) and **(2)** (6.48g, 17.31mmol) were dissolved in THF (80mL). $Pd_2(dba)_3$ (0.396g, 0.432 mmol) and trifurylphosphine (0.501g, 2.16 mmol) were added to reaction mixture and the mixture was stirred for 1 day at 60°C. After crude was extracted with toluene, combined organic layer was dried over $MgSO_4$ and filtrated organic layer was evaporated under reduced pressure. And then, the mixture was purified by a silica gel column chromatography with toluene and hexane. Finally, colorless solid was gained at 64% yield. ^{1}H NMR (400 MHz, $CDCl_3$) δ 7.86 (d, 1H, J = 4.0 Hz), 7.39 (d, 1H, J = 4.0 Hz), 7.34 (d, 1H, J = 8.0 Hz), 7.08 (d, 1H, J = 4.0 Hz).
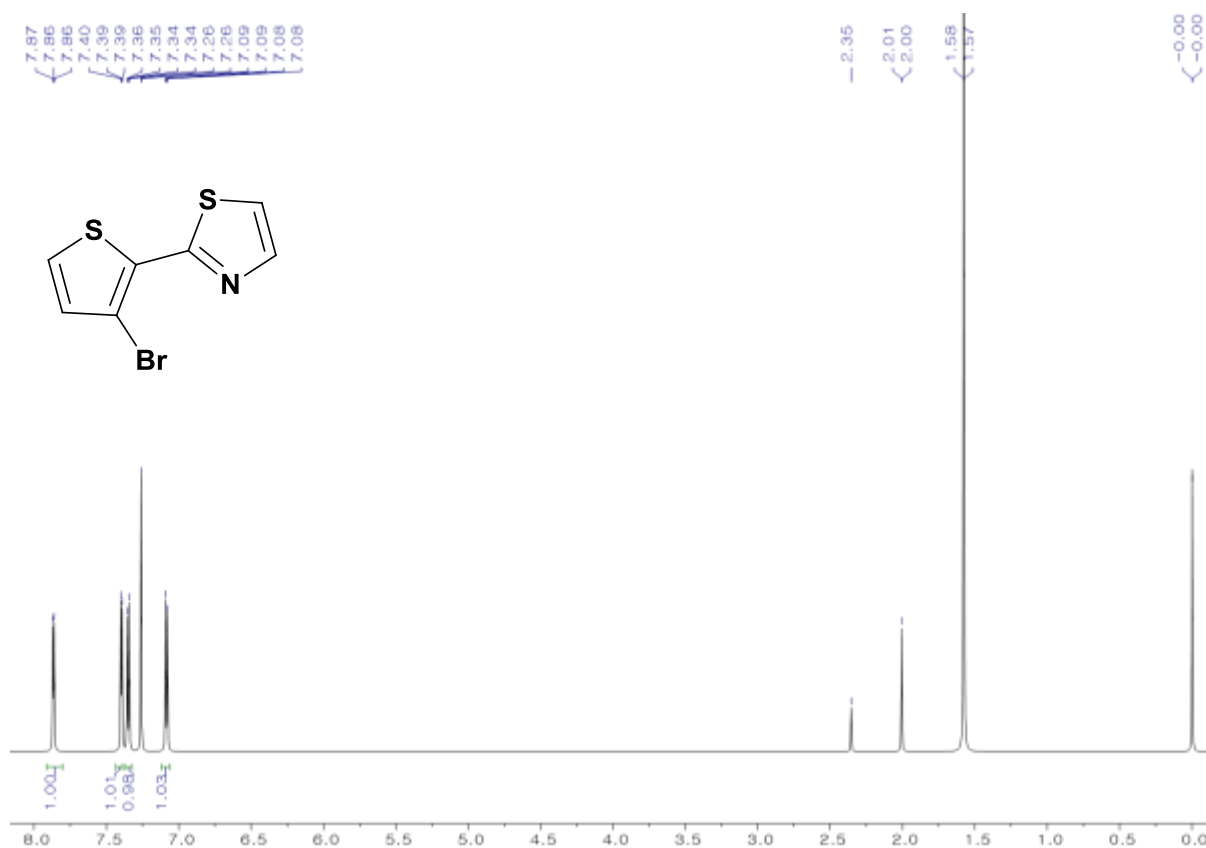
Figure 31. ^{1}H NMR spectra of 2-(3-Bromo-2-thienyl)thiazole.

Synthesis of 2-(3-Dimesitylboryl-2-thienyl)thiazole (**4**): the reaction mixture of 2-(3-bromo-2-thienyl)thiazole (**3**) (0.700 g, 2.84 mmol) in ether (60 mL) was cooled at –78 °C. *n*-BuLi (1.60 M in hexane, 1.78 mL, 2.84 mmol) was added into the reaction mixture. After the mixture was stirred at –78 °C for 1.5 h, dimesitylfluoroborane (0.761 g, 2.84 mmol) dissolving in ether was added to the mixture. The reaction mixture was gradually warmed to room temperature and stirred for 2 h. The mixture was purified by a silica gel column chromatography with hexane and chloroform. Pale-yellow solid was acquired at 75% yield. ^{1}H NMR (400 MHz, CDCl$_3$) δ 7.73 (d, 1H, J = 4.0 Hz), 7.46 (d, 1H, J = 4.0 Hz), 7.25 (d, 1H, J = 4.0 Hz), 6.95 (d, 1H, J = 4.0 Hz), 6.68 (s, 4H), 2.16 (s, 6H), 1.88 (s, 12H).
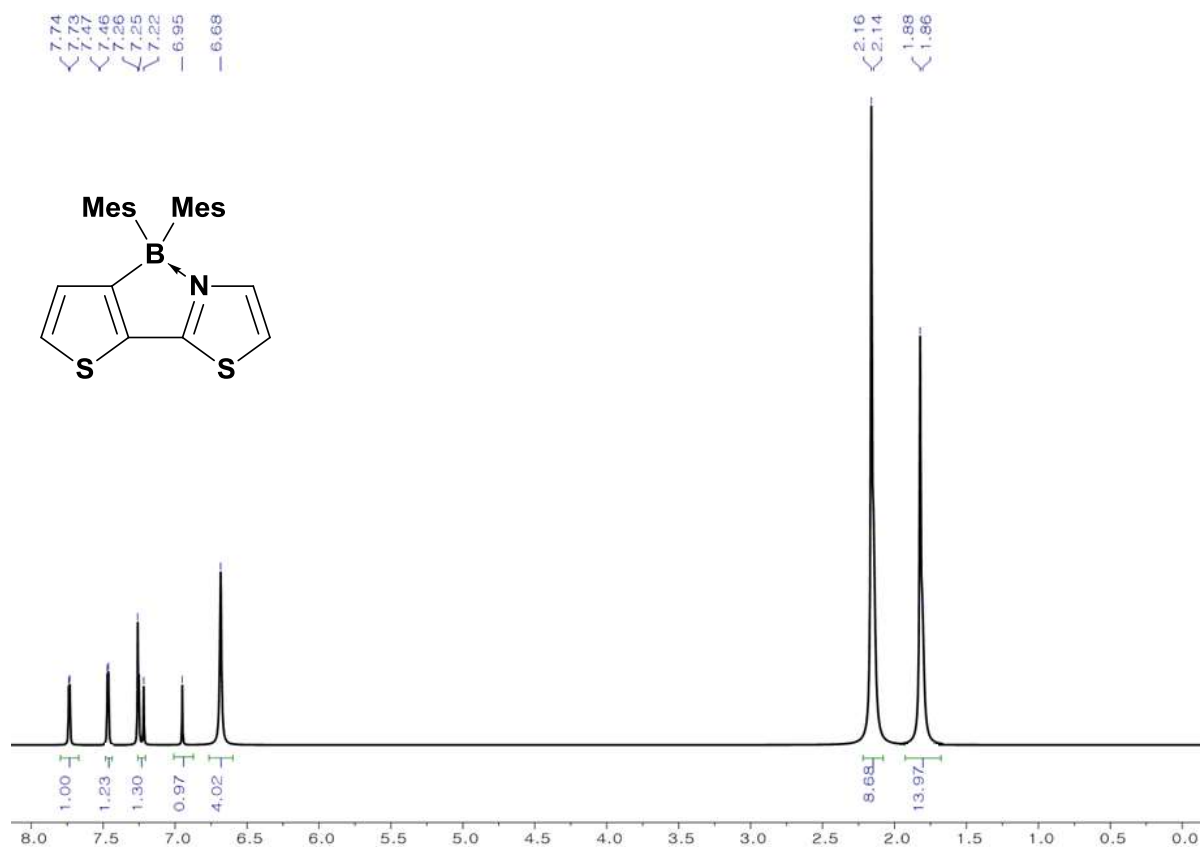
Figure 32. ^{1}H NMR spectra of 2-(3-Dimesitylboryl-2-thienyl)thiazole.

Chapter Ⅳ. References

1.   MacDiarmid, A. G., "Synthetic metals": A novel role for organic polymers (Nobel lecture). *Angew. Chem. Int. Ed.* **2001,** *40* (14), 2581-2590.

2.   (a) Burroughes, J.; Bradley, D.; Brown, A.; Marks, R.; Mackay, K.; Friend, R.; Burns, P.; Holmes, A., Light-emitting diodes based on conjugated polymers. *Nature* **1990,** *347* (6293), 539-541; (b) Kippelen, B.; Brédas, J.-L., Organic photovoltaics. *Energy. Environ. Sci.* **2009,** *2* (3), 251-261; (c) Lin, Y.; Li, Y.; Zhan, X., Small molecule semiconductors for high-efficiency organic photovoltaics. *Chem. Soc. Rev.* **2012,** *41* (11), 4245-4272; (d) Sun, Y.; Welch, G. C.; Leong, W. L.; Takacs, C. J.; Bazan, G. C.; Heeger, A. J., Solution-processed small-molecule solar cells with 6.7% efficiency. *Nat. Mater.* **2012,** *11* (1), 44-48; (e) Wang, C.; Dong, H.; Hu, W.; Liu, Y.; Zhu, D., Semiconducting π-conjugated systems in field-effect transistors: a material odyssey of organic electronics. *Chem. Rev.* **2011,** *112* (4), 2208-2267; (f) Wu, W.; Liu, Y.; Zhu, D., π-Conjugated molecules with fused rings for organic field-effect transistors: design, synthesis and applications. *Chem. Soc. Rev.* **2010,** *39* (5), 1489-1502.

3.   (a) Hou, J.; Park, M.-H.; Zhang, S.; Yao, Y.; Chen, L.-M.; Li, J.-H.; Yang, Y., Bandgap and molecular energy level control of conjugated polymer photovoltaic materials based on benzo [1, 2-b: 4, 5-b′] dithiophene. *Macromolecules* **2008,** *41* (16), 6012-6018; (b) Mas-Torrent, M.; Rovira, C., Novel small molecules for organic field-effect transistors: towards processability and high performance. *Chem. Soc. Rev.* **2008,** *37* (4), 827-838; (c) Roncali, J., Molecular engineering of the band gap of π-conjugated systems: Facing technological applications. *Macromol. Rapid Commun.* **2007,** *28* (17), 1761-1775; (d) Ye, L.; Zhang, S.; Huo, L.; Zhang, M.; Hou, J., Molecular design toward highly efficient photovoltaic polymers based on two-dimensional conjugated benzodithiophene. *Acc. Chem. Res.* **2014,** *47* (5), 1595-1603; (e) Yuan, W. Z.; Gong, Y.; Chen, S.; Shen, X. Y.; Lam, J. W.; Lu, P.; Lu, Y.; Wang, Z.; Hu, R.; Xie, N., Efficient solid emitters with aggregation-induced emission and intramolecular charge transfer characteristics: molecular design, synthesis, photophysical behaviors, and OLED application. *Chem. Mater.* **2012,** *24* (8), 1518-1528.

4.   Cui, Y.; Yao, H.; Gao, B.; Qin, Y.; Zhang, S.; Yang, B.; He, C.; Xu, B.; Hou, J., Fine Tuned Photoactive and Interconnection Layers for Achieving over 13% Efficiency in a Fullerene-free Tandem Organic Solar Cell. *J. Am. Chem. Soc.* **2017**.

5.   Green, M. A.; Hishikawa, Y.; Warta, W.; Dunlop, E. D.; Levi, D. H.; Hohl-Ebinger, J.; Ho-Baillie, A. W., Solar cell efficiency tables (version 50). *Prog. Photovolt. Res. Appl.* **2017,** *25* (7), 668-676.

6.   (a) Fan, B.; Ying, L.; Wang, Z.; He, B.; Jiang, X.-F.; Huang, F.; Cao, Y., Optimisation of processing solvent and molecular weight for the production of green-solvent-processed all-polymer

solar cells with a power conversion efficiency over 9%. *Energy. Environ. Sci.* **2017,** *10* (5), 1243-1251; (b) Koppe, M.; Brabec, C. J.; Heiml, S.; Schausberger, A.; Duffy, W.; Heeney, M.; McCulloch, I., Influence of molecular weight distribution on the gelation of P3HT and its impact on the photovoltaic performance. *Macromolecules* **2009,** *42* (13), 4661-4666; (c) Peumans, P.; Uchida, S.; Forrest, S. R., Efficient bulk heterojunction photovoltaic cells using small-molecular-weight organic thin films. *Nature* **2003,** *425* (6954), 158-162.

7.   (a) Grossiord, N.; Kroon, J. M.; Andriessen, R.; Blom, P. W., Degradation mechanisms in organic photovoltaic devices. *Org. Electron.* **2012,** *13* (3), 432-456; (b) So, F.; Kondakov, D., Degradation Mechanisms in Small-Molecule and Polymer Organic Light-Emitting Diodes. *Adv. Mater.*   **2010,** *22* (34), 3762-3777; (c) Usta, H.; Risko, C.; Wang, Z.; Huang, H.; Deliomeroglu, M. K.; Zhukhovitskiy, A.; Facchetti, A.; Marks, T. J., Design, synthesis, and characterization of ladder-type molecules and polymers. Air-stable, solution-processable n-channel and ambipolar semiconductors for thin-film transistors via experiment and theory. *J. Am. Chem. Soc.* **2009,** *131* (15), 5586-5608; (d) Weitz, R.; Amsharov, K.; Zschieschang, U.; Burghard, M.; Jansen, M.; Kelsch, M.; Rhamati, B.; Van Aken, P.; Kern, K.; Klauk, H., The importance of grain boundaries for the time-dependent mobility degradation in organic thin-film transistors. *Chem. Mater.* **2009,** *21* (20), 4949-4954.

8.   (a) Conboy, G.; Spencer, H. J.; Angioni, E.; Kanibolotsky, A. L.; Findlay, N. J.; Coles, S. J.; Wilson, C.; Pitak, M. B.; Risko, C.; Coropceanu, V., To bend or not to bend–are heteroatom interactions within conjugated molecules effective in dictating conformation and planarity? *Mater. Horizons.* **2016,** *3* (4), 333-339; (b) Jackson, N. E.; Savoie, B. M.; Kohlstedt, K. L.; Olvera de la Cruz, M.; Schatz, G. C.; Chen, L. X.; Ratner, M. A., Controlling conformations of conjugated polymers and small molecules: The role of nonbonding interactions. *J. Am. Chem. Soc.* **2013,** *135* (28), 10475-10483; (c) Jheng, J. F.; Lai, Y. Y.; Wu, J. S.; Chao, Y. H.; Wang, C. L.; Hsu, C. S., Influences of the Non-Covalent Interaction Strength on Reaching High Solid-State Order and Device Performance of a Low Bandgap Polymer with Axisymmetrical Structural Units. *Adv. Mater.* **2013,** *25* (17), 2445-2451; (d) Zhou, H.; Yang, L.; Stuart, A. C.; Price, S. C.; Liu, S.; You, W., Development of fluorinated benzothiadiazole as a structural unit for a polymer solar cell of 7% efficiency. *Angew. Chem.* **2011,** *123* (13), 3051-3054.

9.   Van Der Poll, T. S.; Love, J. A.; Nguyen, T. Q.; Bazan, G. C., Non-Basic High-Performance Molecules for Solution-Processed Organic Solar Cells. *Adv. Mater.* **2012,** *24* (27), 3646-3649.

10.   Moon, M.; Walker, B.; Lee, J.; Park, S. Y.; Ahn, H.; Kim, T.; Lee, T. H.; Heo, J.; Seo, J. H.; Shin, T. J., Dithienogermole-Containing Small-Molecule Solar Cells with 7.3% Efficiency: In-Depth Study on the Effects of Heteroatom Substitution of Si with Ge. *Adv. Energy Mater.* **2015,** *5* (9).

11.   (a) Marinelli, D.; Fasano, F.; Najjari, B.; Demitri, N.; Bonifazi, D., Borazino-doped polyphenylenes. *J. Am. Chem. Soc.* **2017,** *139* (15), 5503-5519; (b) Wakamiya, A.; Taniguchi, T.; Yamaguchi, S., Intramolecular B–N Coordination as a Scaffold for Electron-Transporting Materials: Synthesis and Properties of Boryl-Substituted Thienylthiazoles. *Angew. Chem. Int. Ed.* **2006,** *45* (19), 3170-3173; (c) Wang, X.-Y.; Narita, A.; Feng, X.; Müllen, K., B2N2-Dibenzo [a, e] pentalenes: Effect of the BN Orientation Pattern on Antiaromaticity and Optoelectronic Properties. *J. Am. Chem. Soc* **2015,** *137* (24), 7668-7671; (d) Zhong, Z.; Wang, X.-Y.; Zhuang, F.-D.; Ai, N.; Wang, J.; Wang, J.-Y.; Pei, J.; Peng, J.; Cao, Y., Curved BN-embedded nanographene for application in organic solar cells. *J. Mater. Chem. A* **2016,** *4* (40), 15420-15425.

12.   Dou, C.; Ding, Z.; Zhang, Z.; Xie, Z.; Liu, J.; Wang, L., Developing Conjugated Polymers with High Electron Affinity by Replacing a C   C Unit with a B← N Unit. *Angew. Chem. Int. Ed.* **2015,** *54* (12), 3648-3652.

13.   (a) Kumar, S.; Thorat, K. G.; Ravikanth, M., Synthesis and Properties of Covalently Linked AzaBODIPY–BODIPY Dyads and AzaBODIPY-(BODIPY) 2 Triads. *J. Org. Chem.* **2017,** *82* (13), 6568-6577; (b) Long, X.; Dou, C.; Liu, J.; Wang, L., Fine-Tuning LUMO Energy Levels of Conjugated Polymers Containing a B← N Unit. *Macromolecules* **2017**; (c) Patalag, L. J.; Ho, L. P.; Jones, P. G.; Werz, D. B., Ethylene-Bridged Oligo-BODIPYs: Access to Intramolecular J-Aggregates and Superfluorophores. *J. Am. Chem. Soc.* **2017,** *139* (42), 15104-15113; (d) Sheng, W.; Cui, J.; Ruan, Z.; Yan, L.; Wu, Q.; Yu, C.; Wei, Y.; Hao, E.; Jiao, L., [a]-Phenanthrene-Fused BF2 Azadipyrromethene (AzaBODIPY) Dyes as Bright Near-Infrared Fluorophores. *J. Org. Chem.* **2017,** *82* (19), 10341-10349; (e) Zhao, N.; Xuan, S.; Zhou, Z.; Fronczek, F. R.; Smith, K. M.; Vicente, M. G. H., Synthesis and Spectroscopic and Cellular Properties of Near-IR [a] Phenanthrene-Fused 4, 4-Difluoro-4-bora-3a, 4a-diaza-s-indacenes. *J. Org. Chem.*   **2017,** *82* (18), 9744-9750.

14.   Cao, J.; Liao, Q.; Du, X.; Chen, J.; Xiao, Z.; Zuo, Q.; Ding, L., A pentacyclic aromatic lactam building block for efficient polymer solar cells. *Energy Environ. Sci* **2013,** *6* (11), 3224-3228.

15.   Chen, M. S.; Lee, O. P.; Niskala, J. R.; Yiu, A. T.; Tassone, C. J.; Schmidt, K.; Beaujuge, P. M.; Onishi, S. S.; Toney, M. F.; Zettl, A., Enhanced solid-state order and field-effect hole mobility through control of nanoscale polymer aggregation. *J. Am. Chem. Soc.* **2013,** *135* (51), 19229-19236.

16.   Kim, G.; Kang, S.-J.; Dutta, G. K.; Han, Y.-K.; Shin, T. J.; Noh, Y.-Y.; Yang, C., A thienoisoindigo-naphthalene polymer with ultrahigh mobility of 14.4 cm2/V· s that substantially exceeds benchmark values for amorphous silicon semiconductors. *J. Am. Chem. Soc.* **2014,** *136* (26), 9477-9483.

17.   Liu, J.; Sun, Y.; Moonsin, P.; Kuik, M.; Proctor, C. M.; Lin, J.; Hsu, B. B.; Promarak, V.; Heeger, A. J.; Nguyen, T. Q., Tri-Diketopyrrolopyrrole Molecular Donor Materials for High-

Performance Solution-Processed Bulk Heterojunction Solar Cells. *Adv. Mater.* **2013,** *25* (41), 5898-5903.

18.　　Ma, Z.; Dang, D.; Tang, Z.; Gedefaw, D.; Bergqvist, J.; Zhu, W.; Mammo, W.; Andersson, M. R.; Inganäs, O.; Zhang, F., A Facile Method to Enhance Photovoltaic Performance of Benzodithiophene-Isoindigo Polymers by Inserting Bithiophene Spacer. *Adv. Energy Mater.* **2014,** *4* (6).

19.　　Naber, R. C.; Tanase, C.; Blom, P. W.; Gelinck, G. H.; Marsman, A. W.; Touwslager, F. J.; Setayesh, S.; De Leeuw, D. M., High-performance solution-processed polymer ferroelectric field-effect transistors. *Nat. Mater.* **2005,** *4* (3), 243-248.

20.　　Schubert, M.; Dolfen, D.; Frisch, J.; Roland, S.; Steyrleuthner, R.; Stiller, B.; Chen, Z.; Scherf, U.; Koch, N.; Facchetti, A., Influence of Aggregation on the Performance of All-Polymer Solar Cells Containing Low-Bandgap Naphthalenediimide Copolymers. *Adv. Energy Mater.* **2012,** *2* (3), 369-380.

21.　　Sun, K.; Xiao, Z.; Lu, S.; Zajaczkowski, W.; Pisula, W.; Hanssen, E.; White, J. M.; Williamson, R. M.; Subbiah, J.; Ouyang, J., A molecular nematic liquid crystalline material for high-performance organic photovoltaics. *Nat. Commun.* **2015,** *6*.

22.　　Sun, Y.; Seifter, J.; Wang, M.; Perez, L. A.; Luo, C.; Bazan, G. C.; Huang, F.; Cao, Y.; Heeger, A. J., Effect of Molecular Order on the Performance of Naphthobisthiadiazole-Based Polymer Solar Cells. *Adv. Energy Mater.* **2014,** *4* (6).

23.　　Troshin, P. A.; Mukhacheva, O. A.; Usluer, Ö.; Goryachev, A. E.; Akkuratov, A. V.; Susarova, D. K.; Dremova, N. N.; Rathgeber, S.; Sariciftci, N. S.; Razumov, V. F., Improved Photovoltaic Performance of PPV-Based Copolymers Using Optimized Fullerene-Based Counterparts. *Adv. Energy Mater.* **2013,** *3* (2), 161-166.

24.　　Chen, J.; Cao, Y., Development of novel conjugated donor polymers for high-efficiency bulk-heterojunction photovoltaic devices. *Acc. Chem. Res.* **2009,** *42* (11), 1709-1718.

25.　　He, B.; Pun, A. B.; Zherebetskyy, D.; Liu, Y.; Liu, F.; Klivansky, L. M.; McGough, A. M.; Zhang, B. A.; Lo, K.; Russell, T. P., New form of an old natural dye: bay-annulated indigo (BAI) as an excellent electron accepting unit for high performance organic semiconductors. *J. Am. Chem. Soc.* **2014,** *136* (42), 15093-15101.

26.　　Kageyama, H.; Ohishi, H.; Tanaka, M.; Ohmori, Y.; Shirota, Y., High-Performance Organic Photovoltaic Devices Using a New Amorphous Molecular Material with High Hole Drift Mobility, Tris [4-(5-phenylthiophen-2-yl) phenyl] amine. *Adv. Funct. Mater.* **2009,** *19* (24), 3948-3955.

27.　　Li, H.; Earmme, T.; Subramaniyan, S.; Jenekhe, S. A., Bis (Naphthalene Imide) diphenylanthrazolines: A new class of electron acceptors for efficient nonfullerene organic solar cells

54

and applicable to multiple donor polymers. *Adv. Energy Mater.* **2015,** *5* (8).

28.   Li, J.-L.; Chai, Y.-F.; Wang, W. V.; Shi, Z.-F.; Xu, Z.-G.; Zhang, H.-L., Pyrazine-fused isoindigo: a new building block for polymer solar cells with high open circuit voltage. *ChemComm.* **2017,** *53* (43), 5882-5885.

29.   Wang, T.; Chen, Y.; Bao, X.; Du, Z.; Guo, J.; Wang, N.; Sun, M.; Yang, R., A new isoindigo-based molecule with ideal energy levels for solution-processable organic solar cells. *Dyes Pigm.* **2013,** *98* (1), 11-16.

30.   Yang, R.; Tian, R.; Hou, Q.; Yang, W.; Cao, Y., Synthesis and optical and electroluminescent properties of novel conjugated copolymers derived from fluorene and benzoselenadiazole. *Macromolecules* **2003,** *36* (20), 7453-7460.

31.   Zyung, T.; Hwang, D.-H.; Kang, I.-N.; Shim, H.-K.; Hwang, W.-Y.; Kim, J.-J., Novel blue electroluminescent polymers with well-defined conjugation length. *Chem. Mater.* **1995,** *7* (8), 1499-1503.

32.   Bin, H.; Gao, L.; Zhang, Z.-G.; Yang, Y.; Zhang, Y.; Zhang, C.; Chen, S.; Xue, L.; Yang, C.; Xiao, M., 11.4% Efficiency non-fullerene polymer solar cells with trialkylsilyl substituted 2D-conjugated polymer as donor. *Nat. Commun.* **2016,** *7*, 13651.

33.   Cui, C.; Wong, W. Y., Effects of alkylthio and alkoxy side chains in polymer donor materials for organic solar cells. *Macromol. Rapid. Commun.* **2016,** *37* (4), 287-302.

34.   Feng, S.; Liu, C.; Xu, X.; Liu, X.; Zhang, L.; Nian, Y.; Cao, Y.; Chen, J., Siloxane-Terminated Side Chain Engineering of Acceptor Polymers Leading to Over 7% Power Conversion Efficiencies in All-Polymer Solar Cells. *ACS Macro Lett.* **2017,** *6*, 1310-1314.

35.   Han, A.-R.; Lee, J.; Lee, H. R.; Lee, J.; Kang, S.-H.; Ahn, H.; Shin, T. J.; Oh, J. H.; Yang, C., Siloxane side chains: a universal tool for practical applications of organic field-effect transistors. *Macromolecules* **2016,** *49* (10), 3739-3748.

36.   Huang, W.; Li, M.; Zhang, L.; Yang, T.; Zhang, Z.; Zeng, H.; Zhang, X.; Dang, L.; Liang, Y., Molecular engineering on conjugated side chain for polymer solar cells with improved efficiency and accessibility. *Chem. Mater.* **2016,** *28* (16), 5887-5895.

37.   Lee, J.; Han, A.-R.; Yu, H.; Shin, T. J.; Yang, C.; Oh, J. H., Boosting the ambipolar performance of solution-processable polymer semiconductors via hybrid side-chain engineering. *J. Am. Chem. Soc.* **2013,** *135* (25), 9540-9547.

38.   Lin, Y.; Zhao, F.; He, Q.; Huo, L.; Wu, Y.; Parker, T. C.; Ma, W.; Sun, Y.; Wang, C.; Zhu, D., High-performance electron acceptor with thienyl side chains for organic photovoltaics. *J. Am. Chem. Soc.* **2016,** *138* (14), 4955-4961.

39.   Yang, Y.; Zhang, Z.-G.; Bin, H.; Chen, S.; Gao, L.; Xue, L.; Yang, C.; Li, Y., Side-chain

isomerization on an n-type organic semiconductor ITIC acceptor makes 11.77% high efficiency polymer solar cells. *J. Am. Chem. Soc.* **2016,** *138* (45), 15011-15018.

40.   Fronk, S. L.; Wang, M.; Ford, M.; Coughlin, J.; Mai, C.-K.; Bazan, G. C., Effect of chiral 2-ethylhexyl side chains on chiroptical properties of the narrow bandgap conjugated polymers PCPDTBT and PCDTPT. *Chem. Sci.* **2016,** *7* (8), 5313-5321.

41.   Gevaerts, V. S.; Herzig, E. M.; Kirkus, M.; Hendriks, K. H.; Wienk, M. M.; Perlich, J.; Müller-Buschbaum, P.; Janssen, R. A., Influence of the position of the side chain on crystallization and solar cell performance of DPP-based small molecules. *Chem. Mater.* **2013,** *26* (2), 916-926.

42.   Henze, O.; Feast, W. J.; Gardebien, F.; Jonkheijm, P.; Lazzaroni, R.; Leclère, P.; Meijer, E.; Schenning, A. P., Chiral Amphiphilic Self-Assembled α, α '-Linked Quinque-, Sexi-, and Septithiophenes: Synthesis, Stability and Odd− Even Effects.*J. Am. Chem. Soc.* **2006,** *128* (17), 5923-5929.

43.   Livi, F.; Zawacka, N. K.; Angmo, D.; Jørgensen, M.; Krebs, F. C.; Bundgaard, E., Influence of side chain position on the electrical properties of organic solar cells based on dithienylbenzothiadiazole-alt-phenylene conjugated polymers. *Macromolecules* **2015,** *48* (11), 3481-3492.

44.   Rumer, J. W.; Hor, C. K.; Meager, I.; Yau, C. P.; Huang, Z.; Nielsen, C. B.; Watkins, S. E.; Bronstein, H.; McCulloch, I., Alkyl side-chain branching point effects in thieno [3, 4-c] pyrrole-4, 6-dione copolymers. *Journal of Organic Semiconductors* **2013,** *1* (1), 30-35.

45.   Zerdan, R. B.; Shewmon, N. T.; Zhu, Y.; Mudrick, J. P.; Chesney, K. J.; Xue, J.; Castellano, R. K., The influence of solubilizing chain stereochemistry on small molecule photovoltaics. *Adv. Funct. Mater.* **2014,** *24* (38), 5993-6004.

46.   Melucci, M.; Favaretto, L.; Zanelli, A.; Cavallini, M.; Bongini, A.; Maccagnani, P.; Ostoja, P.; Derue, G.; Lazzaroni, R.; Barbarella, G., Thiophene–Benzothiadiazole Co-Oligomers: Synthesis, Optoelectronic Properties, Electrical Characterization, and Thin-Film Patterning. *Adv. Funct. Mater.* **2010,** *20* (3), 445-452.

47.   Han, L.; Jiang, H.; Ouyang, D.; Chen, W.; Hu, T.; Wang, J.; Wen, S.; Sun, M.; Yang, R., Cyclic alkyl chains promote the polymer self-assembly and packing orders for solar cells. *Nano Energy* **2017,** *36*, 110-117.

48.   Huang, H.; Youn, J.; Ponce Ortiz, R.; Zheng, Y.; Facchetti, A.; Marks, T., Very large silacylic substituent effects on response in silole-based polymer transistors. *Chem. Mater.***2011,** *23* (8), 2185-2200.

59.   Locklin, J.; Li, D.; Mannsfeld, S. C.; Borkent, E.-J.; Meng, H.; Advincula, R.; Bao, Z., Organic thin film transistors based on cyclohexyl-substituted organic semiconductors. *Chem. Mater.*

2005, *17* (13), 3366-3374.

50.   Ren, G.; Ahmed, E.; Jenekhe, S. A., Non-Fullerene Acceptor-Based Bulk Heterojunction Polymer Solar Cells: Engineering the Nanomorphology via Processing Additives. *Adv. Energy Mater.* **2011,** *1* (5), 946-953.

51.   Schwenn, P. E.; Gui, K.; Nardes, A. M.; Krueger, K. B.; Lee, K. H.; Mutkins, K.; Rubinstein-Dunlop, H.; Shaw, P. E.; Kopidakis, N.; Burn, P. L., A Small Molecule Non-fullerene Electron Acceptor for Organic Solar Cells. *Adv. Energy Mater.* **2011,** *1* (1), 73-81.

52.   Sun, D.; Meng, D.; Cai, Y.; Fan, B.; Li, Y.; Jiang, W.; Huo, L.; Sun, Y.; Wang, Z., Non-fullerene-acceptor-based bulk-heterojunction organic solar cells with efficiency over 7%. *J. Am. Chem. Soc.* **2015,** *137* (34), 11156-11162.

53.   Wang, M.; Hu, X.; Liu, P.; Li, W.; Gong, X.; Huang, F.; Cao, Y., Donor–acceptor conjugated polymer based on naphtho [1, 2-c: 5, 6-c] bis [1, 2, 5] thiadiazole for high-performance polymer solar cells. *J. Am. Chem. Soc.* **2011,** *133* (25), 9638-9641.

54.   Zhao, W.; Qian, D.; Zhang, S.; Li, S.; Inganäs, O.; Gao, F.; Hou, J., Fullerene-Free Polymer Solar Cells with over 11% Efficiency and Excellent Thermal Stability. *Adv. Mater.* **2016,** *28* (23), 4734-4739.

55.   Zhou, H.; Yang, L.; Stuart, A. C.; Price, S. C.; Liu, S.; You, W., Development of fluorinated benzothiadiazole as a structural unit for a polymer solar cell of 7% efficiency. *Angew. Chem.***2011,** *123* (13), 3051-3054.

56.   Jung, J. W.; Russell, T. P.; Jo, W. H., A small molecule composed of dithienopyran and diketopyrrolopyrrole as versatile electron donor compatible with both fullerene and nonfullerene electron acceptors for high performance organic solar cells. *Chem. Mater.* **2015,** *27* (13), 4865-4870.

57.   Walker, B.; Han, D.; Moon, M.; Park, S. Y.; Kim, K.-H.; Kim, J. Y.; Yang, C., Effect of Heterocyclic Anchoring Sequence on the Properties of Dithienogermole-Based Solar Cells. *ACS Appl. Mater. Interfaces* **2017,** *9* (8), 7091-7099.

58.   Moon, M.; Walker, B.; Lee, J.; Park, S. Y.; Ahn, H.; Kim, T.; Lee, T. H.; Heo, J.; Seo, J. H.; Shin, T. J., Dithienogermole-Containing Small-Molecule Solar Cells with 7.3% Efficiency: In-Depth Study on the Effects of Heteroatom Substitution of Si with Ge. *Adv. Enegy Mater.* **2015,** *5* (9).

59.   Han, L.; Chen, W.; Hu, T.; Ren, J.; Qiu, M.; Zhou, Y.; Zhu, D.; Wang, N.; Sun, M.; Yang, R., Intra-and Intermolecular Steric Hindrance Effects Induced Higher Open-Circuit Voltage and Power Conversion Efficiency. *ACS Macro Lett.* **2015,** *4* (4), 361-366.

60.   Wen, S.; Chen, W.; Fan, M.; Duan, L.; Qiu, M.; Sun, M.; Han, L.; Yang, R., A diketopyrrolopyrrole-based low bandgap polymer with enhanced photovoltaic performances through backbone twisting. *J. Mater. Chem. A* **2016,** *4* (46), 18174-18180.

61.   Andersson, M. R.; Berggren, M.; Inganäs, O.; Gustafsson, G.; Gustafsson-Carlberg, J.; Selse, D.; Hjertberg, T.; Wennerström, O., Electroluminescence from substituted poly (thiophenes): from blue to near-infrared. *Macromolecules* **1995,** *28* (22), 7525-7529.

62.   Sun, Y.; Seifter, J.; Huo, L.; Yang, Y.; Hsu, B. B.; Zhou, H.; Sun, X.; Xiao, S.; Jiang, L.; Heeger, A. J., High-Performance Solution-Processed Small-Molecule Solar Cells Based on a Dithienogermole-Containing Molecular Donor. *Adv. Energy Mater.* **2015,** *5* (3).

63.   Shoji, H.; Kitagawa, D.; Kobatake, S., Alkyl substituent effects in photochemical and thermal reactions of photochromic thiophene-S, S-dioxidized diarylethenes. *New. J. Chem.* **2014,** *38* (3), 933-941.

64.   (a) Blom, P. W.; Mihailetchi, V. D.; Koster, L. J. A.; Markov, D. E., Device physics of polymer: fullerene bulk heterojunction solar cells. *Adv. Mater.* **2007,** *19* (12), 1551-1566; (b) Boudreault, P.-L. T.; Najari, A.; `Leclerc, M., Processable low-bandgap polymers for photovoltaic applications. *Chem. Mater.* **2010,** *23* (3), 456-469; (c) Bureš, F., Fundamental aspects of property tuning in push–pull molecules. *RSC Adv.* **2014,** *4* (102), 58826-58851; (d) Duan, C.; Huang, F.; Cao, Y., Recent development of push–pull conjugated polymers for bulk-heterojunction photovoltaics: rational design and fine tailoring of molecular structures. *J. Mater. Chem.* **2012,** *22* (21), 10416-10434.

65.   (a) Efrem, A.; Wang, K.; Jia, T.; Wang, M., Direct arylation polymerization toward a narrow bandgap donor–acceptor conjugated polymer of alternating 5, 6-difluoro-2, 1, 3-benzothiadiazole and alkyl-quarternarythiophene: From synthesis, optoelectronic properties to devices. *Journal of Polymer Science Part A: Polym. Chem.* **2017,** *55* (11), 1869-1879; (b) Nketia-Yawson, B.; Lee, H. S.; Seo, D.; Yoon, Y.; Park, W. T.; Kwak, K.; Son, H. J.; Kim, B.; Noh, Y. Y., A Highly Planar Fluorinated Benzothiadiazole-Based Conjugated Polymer for High-Performance Organic Thin-Film Transistors. *Adv. Mater.* **2015,** *27* (19), 3045-3052; (c) You, J.; Chen, C. C.; Hong, Z.; Yoshimura, K.; Ohya, K.; Xu, R.; Ye, S.; Gao, J.; Li, G.; Yang, Y., 10.2% power conversion efficiency polymer tandem solar cells consisting of two identical sub-cells. *Adv. Mater.* **2013,** *25* (29), 3973-3978; (d) You, J.; Dou, L.; Yoshimura, K.; Kato, T.; Ohya, K.; Moriarty, T.; Emery, K.; Chen, C.-C.; Gao, J.; Li, G., A polymer tandem solar cell with 10.6% power conversion efficiency. *Nat. Commun.* **2013,** *4*, 1446.

66.   Carsten, B.; Szarko, J. M.; Son, H. J.; Wang, W.; Lu, L.; He, F.; Rolczynski, B. S.; Lou, S. J.; Chen, L. X.; Yu, L., Examining the effect of the dipole moment on charge separation in donor–acceptor polymers for organic photovoltaic applications. *J. Am. Chem. Soc.* **2011,** *133* (50), 20468-20475.

67.   Eperon, G. E.; Burlakov, V. M.; Docampo, P.; Goriely, A.; Snaith, H. J., Morphological control for high performance, solution-processed planar heterojunction perovskite solar cells. *Adv.*

Funct. Mater. **2014,** *24* (1), 151-157.

Acknowledgment

감사의 글

저에게 있어 연구에 대한 부푼 꿈을 안고 UNIST에 진학은 큰 행운이자 또다른 성장의 기회였습니다. 무사히 학위기간을 맞출 수 있게 도움을 주었던 모든 분께 감사의 말을 전하는 바입니다.

가장 먼저 학위기간동안 저에게 보다 넓은 연구에 대한 안목만이 아니라, 때로는 인생에 대한 조언까지도 아껴 주시지 않은 저의 지도 교수님 양창덕 교수님께 진심으로 감사드립니다. 비단 저에게 있어서는 지도 교수님의 의미를 뛰어넘어 제가 또다른 환경에서 잘 생활해 나갈 수 있도록 도움을 주신만큼, 기대에 부흥하는, 어디서도 제 역할을 당당히 해 나갈 수 있는 ATOMS의 일원이 되도록 하겠습니다.

또한 우리 ATOMS 식구들에게 말로는 표현 못했지만 많은 도움 그리고 힘이 되주어서 진심으로 감사드립니다. 앞으로도 ATOMS의 행보에 항상 좋은 일과 행복한 나날들이 계속되도록 응원하겠습니다.

나의 절친들 기영이 현복이 민준이 늘 응원해주고 믿어주어서 정말 고맙고 앞으로도 너희의 자랑스런 친구이자 각자의 위치에서 최선을 다하는 사람이 되도록 하자.

마지막으로 항상 저를 묵묵히 응원 해 주시던 부모님, 누나 진심으로 감사드리고 사랑합니다. 앞으로 자랑스러운 아들, 동생이 될 수 있도록 노력하겠습니다.

Publication List

1. Bright Walker, **Daehee Han**, Mijin Moon, Song Yi Park, Ka-Hyun Kim, Jin Young Kim and Changduk Yang "Effect of Heterocyclic Anchoring Sequence on the Properties of Dithienogermole-based Solar Cells", *ACS Appl. Mater. Interfaces.*, 2017, 9, 7091

2. Jihoon Lee, Vellaiappillai Tamilavan, Kyung Hwan Rho, Sangha Keum, Ki Hong Park, **Daehee han**, Yun Kyung Jung, Changduk Yang, Youngeup Jin, Jae-Won Jang, Jung Hyun Jeong, Sung Heum Park "Overcoming Fill Factor Reduction in Ternary Polymer Solar Cells by Matching the Highest Occupied Molecular Orbital Energy Levels of Donor Polymers", *Adv. Energy Mater.*, 2017, 1702251

3. Yujin An, Jiyeon Oh, Shanshan Chen, Byongkyu Lee, Sang Myeon Lee, **Daehee Han**, and Changduk Yang, "Effect of incorporating different chalcogenophene comonomers into random acceptor terpolymers on the morphology and performance of all-polymer solar cells", submitted

4. **Daehee Han**, Tanya Kumari, Yujin An, Sungwoo Jung, and Changduk Yang, "A comparative investigation of cyclohexyl-end-capped versus hexyl-end-capped small-molecule donors on small donor:polymer acceptor junction solar cells", submitted